INSTRUMENTATION OF A DIESEL ENGINE FOR OIL FILM THICKNESS MEASUREMENTS USING FIBER OPTICS AND LASER FLUORESCENCE

by

EDWARD N. INGLES
B.S. Mechanical Engineering, University of Michigan
(1984)

SUBMITTED TO THE DEPARTMENT OF
OCEAN ENGINEERING
IN PARTIAL FULFILLMENT OF THE REQUIREMENTS
FOR THE DEGREES OF
NAVAL ENGINEER

and

MASTER OF SCIENCE IN MECHANICAL ENGINEERING

at the

MASSACHUSETTS INSTITUTE OF TECHNOLOGY
June,1991

INSTRUMENTATION OF A DIESEL ENGINE FOR OIL FILM THICKNESS MEASUREMENTS USING FIBER OPTICS AND LASER FLUORESCENCE

by

EDWARD N. INGLES

Submitted to the Department of Ocean Engineering on May 10, 1991 in partial fulfillment of the requirements for the degrees of Naval Engineer and Master of Science in Mechanical Engineering.

ABSTRACT

An apparatus was designed to measure the oil film thickness in a production diesel engine using the laser fluorescence technique. The apparatus incorporated fiber optic technology in its design in an attempt to improve on the ease of installation, portability, durability, and signal to noise ratio of previous designs using conventional optics.

Bench tests and operational tests were conducted to evaluate the performance of the design. These tests indicate that the goals of the design were achieved, with a signal to noise ratio of the new design comparable to that of the conventional optics design.

Thesis supervisor: David P. Hoult

Title: Senior Research Associate
Department of Mechanical Engineering

ACKNOWLEDGEMENTS

I would like to thank my thesis supervisor Dr. David Hoult for the opportunity to conduct this research and for guidance during the course of this project. I would also like to thank the following people associated with Sloan Automotive Laboratory for their support during the course of this research: Dr. Victor Wong, Don Fitzgerald, Brian Corkum, Gayle Ivey, Tim Cherry, Byron Shaw, Dean Moon, Dennis Logan, Jim Azzola, and Matt Bliven.

I also wish to thank Lori Van Amburgh for her encouragement and support during the course of this challenging yet personally rewarding research.

This work was sponsored by the MIT Consortium on Lubrication in Internal Combustion Engines at the Sloan Automotive Laboratory. Members include Ford Motor Co., Pennzoil Products Co., PSA/Renault, Sealed Power Inc., the National Institute of Standards and Testing, and the U.S. Department of Energy.

TABLE OF CONTENTS

LIST OF FIGURES

1. INTRODUCTION

Numerous researchers have used the laser fluorescence technique to measure lubricating oil film thicknesses in operating internal combustion engines [1,2,3]. These efforts have typically used conventional optics to guide the incident laser beam onto the oil film and to collect the resulting fluorescence signal. While useful results can be obtained using conventional optics, there are several drawbacks to using this technology. These drawbacks include:

1. laborious initial alignment of the optics
2. large area required for setting up the optical train
3. proximity of the system to the engine, resulting in high vibration noise in the output of the detector, degradation in laser power over time, and misalignment of the optics due to vibration
4. realignment of the optics for each engine studied
5. requirement for a clear optical path from the exterior of the engine to the liner surface
6. low laser power incident on the oil film due to optical losses.

The goal of this research was to replace the conventional optics of previous research efforts with fiber optics. By making this conversion, it was anticipated that the following improvements could be made:

1. installation of the laser fluorescence apparatus would be made less difficult and time consuming
2. the apparatus would be made portable and more compact
3. the system would be less vulnerable to engine vibration
4. the apparatus would be less engine specific
5. elimination of the requirement for a clear optical path
6. increased signal to noise ratio due to higher incident laser power on the oil film.

2. DESIGN CONSTRAINTS

The application of the laser fluorescence technique to oil film thickness measurements in a running engine entails several constraints that drive the design of the apparatus. These constraints can be divided into three categories: environmental constraints, physical constraints, and those constraints resulting from the requirements of the laser fluorescence technique itself.

Environmental constraints on the design result from the fact that some of the components of the apparatus must operate within the block of the running engine. Within the block, temperatures range from approximately 150 C at the liner-coolant interface, to approximately 90 C in the coolant itself. Circulating coolant in the block makes it imperative that components within the block are watertight. The running engine also has a vibrational amplitude of several mm, requiring the components of the system within the engine to be resistant to vibratory misalignment.

Physical constraints involve placing the required system components in their proper positions on the cylinder liner and at the proper focal length without excessively disrupting the normal operation of the engine. Since most engines are quite compact, this constraint introduces considerable difficulty into the design. In addition, it was decided early in the project to use standard components wherever possible. This restriction is significant in that most available components are larger than desired.

The third type of constraint involves obtaining satisfactory system parameters to successfully apply the laser fluorescence technique. The most critical of these parameters are laser power incident on the oil film, the size of the spot illuminated by the laser, and signal to noise ratio.

3. LASER FLUORESCENCE THEORY

The laser fluorescence technique for measuring oil film thickness exploits the fact that fluorescent dyes when excited by laser light of a certain wavelength will emit light at a second wavelength. A detailed explanation of the laser fluorescence phenomenon is contained in [4]. There are several characteristics of this phenomenon worth noting here.

The intensity of the emitted fluorescence is linear with film thickness for films less than 125 um and low dye concentrations [5]. In this engine, film thicknesses of interest (i.e. those in the vicinity of the ring pack) are within this range. The chosen fluorescent dye, Coumarin 523, is added to the oil in a 10**-4 mol/liter concentration, after mixing with a dichloromethane solvent. This dye emits fluorescence with a spectral peak at approximately 500 nm when excited by light at 442 nm. This concentration meets the requirements for linearity and is low enough to not adversely affect the additive package of the oils being tested.

The emitted fluorescence of the oil decreases with increasing temperature. This effect was studied in detail by Hoult and Takaguchi [6]. This characteristic, known as the "bleach" effect, makes it necessary to have an incident beam diameter smaller than the smallest feature being studied on the engine, in order to ensure that fresh oil is scraped into the incident beam on each stroke [5]. For this engine, the smallest feature corresponds to the width of the piston rings. Since the beam diameter in the apparatus developed in this project is approximately 50 μm, compared to ring widths on the order of 1 mm, this requirement is met. This effect also is encountered during bench testing, where the oil in the test piece must either be circulated or allowed to cool after each reading to prevent local heating of the oil from affecting the fluorescence measurement.

4. FIBER OPTICS PRINCIPLES AND TERMINOLOGY

This section is included in order to familiarize the reader with the terminology and basic concepts of fiber optics. Only those concepts which directly affected the development of this apparatus will be discussed.

Optical fibers act as "light pipes", channeling light along a desired path by reflecting the light off of a reflective material that surrounds a transparent core. The properties of the transparent fiber material and the reflective material surrounding the fiber, called cladding, determine the characteristics of the fiber. The most important characteristic for this application is the emergence/ acceptance angle. Optical fibers only accept light that strikes the end of the fiber within a certain conical angle called the acceptance angle. Light striking the fiber at angles greater than the acceptance angle will not be transmitted. Likewise, as light exits the fiber, it emerges at the same angle, here referred to as the emergence angle. For the silica core fibers used in this system, the acceptance/emergence angle is approximately 25 degrees.

The acceptance angle is important when coupling the laser beam into the fiber. In this application, the diameter of the fiber is 50 μm, while the diameter of the laser beam is 1 mm. Some focusing is required to couple the beam into the fiber, but the focusing must be done in such a way as to have the laser beam incident on the fiber within the acceptance angle. The acceptance angle is also important in the collection of fluorescent signal, as it determines the solid angle within which the fluorescence must fall to be collected.

The emergence angle is crucial in this application because the light emerging from the fiber diverges rapidly from its initial diameter of 50 μm, and has a diameter greater than the maximum desired spot size of 100 μm at a distance of only 113 μm (Fig 1). Since the light must travel through the thickness of the liner to reach the oil, clearly some focusing optics at the engine end of the illumination fiber are required in order to provide a sufficiently small spot at the inner liner surface.

Emergence angle also plays a role at the detector end of the apparatus. Either the output of the system must be collimated before it is filtered and strikes the photomultiplier head, or some loss in signal strength and some enlarging and shifting of the bandpass of installed filters must be accepted.

Optical fibers exhibit extremely low transmission loss, and for the distances involved in this application these losses are negligible. This low transmission loss is a substantial improvement over the conventional optical train, which had an overall efficiency of approximately 30%, and allows the fiber optic system to put more laser power on the film with no increase in power at the laser aperture.

5. DESCRIPTION OF APPARATUS

The laser source for the apparatus is a 17 mW Liconix 4214NB HeCd laser operating in the blue at 442 nm. While this laser has a very narrow peak at 442 nm, some power is found in the tails of the laser at wavelengths away from 442 nm. Components of the laser output near the fluorescence peak at 500 nm can cause noise in the system output.

The laser is coupled into an optical fiber using an eccentric coupler (Fig 2). This coupler is a standard commercially available component. The coupler works by aligning a

focusing lens between the laser and the end of the optical fiber. Coupling efficiencies are typically in the range of 50% for the fiber core diameter used in this apparatus.

Three optical cables were developed and evaluated for use in this application. The optical cable used in the final configuration consists of one 50 μm diameter silica fiber to transmit the laser light to the oil film, surrounded by eighteen 100 μm diameter silica fibers to collect and transmit the fluorescent signal. The cable is bifurcated, a common end with both 50 and 100 μm fibers goes to the engine, while one leg containing the 50 μm illumination fiber goes to the laser and one leg containing only the collection fibers goes to the photomultiplier tube. A diagram showing the flow path of laser light and fluorescent signal in the bifurcated cable can be found in Fig 3. Descriptions of the other two fibers evaluated can be found in appendix 1. The flow diagram for the fused fiber coupler is shown in Fig 4.

At the engine the laser light is concentrated on the oil film by a focusing probe. This probe contains two lenses that collimate and focus the laser light, with a working distance of approximately 12 mm from the end of the probe. A drawing of this probe can be found in Fig 5. The fluorescent signal that is generated by the laser light is collected through this same focusing probe and coupled into the 100 μm fibers, which then transmit the signal to the photomultiplier tube.

Prior to the signal entering the photomultiplier tube, it is filtered to remove any laser reflection that may have entered the collection fibers. This filtering is accomplished with one 500 nm narrowband filter. Specifications for this filter can be found in fig 6.

After filtering, the fluorescent signal is directed onto a photomultiplier tube (PMT), which converts the incoming photons into a weak current, which is then sent to a pre-amplifier for conversion to a voltage signal. The commercially produced pre-amplifier used in the apparatus does not have an optimum time constant for this application. Since the engine is running at very high linear piston speeds, the time constant of the pre-amplifier must be sufficiently short to give good resolution both horizontally and vertically. Previous research efforts used a custom pre-amplifier with an optimum time constant and a gain of 10**6. This amplifier was inoperative due to a malfunctioning IC chip during the culmination of this research, so the less optimal commercial pre-amplifier was used. By operating this pre-amplifier at its minimum time constant and a gain of 10**7, results were obtained that, while not of sufficient quality to be used in detailed analysis of oil film behavior, are adequate to demonstrate the successful operation of the apparatus.

Data acquisition was completely analogous to [1]. Crank angle, bottom dead center (BDC) pulse, PMT output, and cylinder pressure were collected and used to evaluate the performance of the apparatus.

Penetration of the engine block and cylinder liner in order to provide access to the oil film is necessary, and requires careful modification of the engine. The engine modifications must hold the focusing probe normal to the liner surface, they must prevent water from coming between the probe face and the quartz window, and the position of the probe must be adjustable to focus the laser light on the inner surface of the liner.

The modifications to the engine consist of three major components: a quartz window for optical access to the oil film, a radiator insert to give clearance in the engine block for installation of the probe, and a cylindrical holder for the focusing probe. The modified engine is shown in Fig 7. The quartz window and cylinder liner are the same as those used by Bliven. The radiator insert is ~1.5" higher than that used by Bliven, in order to give enough room for insertion and removal of the probe during testing without disassembly of the engine. In future installations this height can be reduced by installing the probe in the probe holder prior to engine assembly. The probe holder (fig 8) is installed in the same position as the optical sight tube used by Bliven, but is completely redesigned to hold the focusing probe and to provide a more repeatable and secure seal at the liner surface. When fully assembled, this fixturing positions the the illuminated spot such that the crown of the piston crosses the incident beam at +- 88 degrees after top center (ATC), rather than +- 81.6 degrees ATC in the case of the previous installation.

The laser, coupler, PMT, and pre-amplifier were removed from the engine test bed and mounted on a wheeled cart, using the optical board and vibration mounts described in [1]. This modification makes the apparatus portable and isolates it from engine vibration, thus eliminating vibration degradation of the laser and vibration noise in the output of the PMT.

6. BENCH TESTING

Bench tests were conducted with three different fiber optic cables and six different combinations of 442 nm and 500 nm filters in order to determine the optimum combination for this application. Filter combination nomenclature is in Fig 9, the test matrix can be seen in Fig 10. Specifications for the 442 nm filters can be found in Fig 6. System noise, fluorescent signal, optimum probe power, and focal length for each combination were measured. Horizontal resolution was measured for the fused fiber coupler (FFC).

The test apparatus developed, shown in Fig 11, uses the chemically etched test pieces developed by Takaguchi [5] in order to provide a uniform oil film thickness. The test pieces are mounted on a micrometer drive that provides axial adjustment for the focusing probe as well as vertical and horizontal adjustment for the test piece.

Three types of noise were measured. SMA noise refers to the output of the PMT with the focusing probe removed and the illumination fiber pointing into space. Probe noise refers to PMT output with the focusing probe installed and pointing into space. Dry reflectance refers to the PMT output when the laser is focused on a dry test piece. This is a measure of both the reflection off the aluminum test piece and the quartz window of the test piece. These surfaces closely approximate the piston and liner window surfaces. It should be noted that this measurement of reflectance is a worst case, since it can be assumed that the oil will absorb some of the reflected, as well as some of the incident, laser light.

In measuring the fluorescent signal collected by each combination, six readings were taken at different locations on the test piece. These readings were taken at three minute intervals. These steps were necessary to ensure that local heating of the oil did not cause bleaching of the fluorescent signal, and that the readings reflected the average depth of the test piece.

Probe power was measured for each combination prior to taking measurements in order to put the data collected on a per mW of probe power basis for comparison. In addition, the optimum probe power for zero, one, and two 442 nm filters was measured.

The focal length of each cable/probe combination is different due to slight variations in the centering of the illumination fiber and the emergence angle. Each cable/probe combination must be evaluated while properly focused. Focal length for each cable/probe

combination was measured by maximizing the dry reflectance of the combination through axial adjustment of the probe.

Horizontal resolution for the 50 μm fiber was tested using the FFC and the test apparatus. By scanning the illuminated spot across the outer edge of the etched depression of the test piece and comparing the result with an etch mark profile obtained using a profilometer, the resolution of the system can be judged.

All noise and signal data for the fused fiber coupler was collected with a PMT gain of 10**8. Data for the bifurcated cables was collected with a PMT gain of 10**6.

7. BENCH TEST ANALYSIS

Noise data for each combination can be found in Figs 12-15. The FFC has a significant amount of SMA noise due to its direct path for the laser to follow to the PMT. The bifurcated cables have negligible SMA noise due to their separate laser and signal paths.Probe noise for all the combinations was zero, showing that internal reflection from the focusing probe was not a concern. Dry reflectance is significant in the bifurcated cables, but negligible in the FFC due to its poor collection efficiency compared with the bifurcated cables.

Fluorescent signal data for the combinations can be found in figs 16-19. The magnitude of the fluorescent signal collected by the FFC is only 1% of that collected by the bifurcated cables, with roughly equivalent probe power. This is due to the same inefficient collection noted in the dry reflectance measurements. The uncollimated cables had a higher signal level than the collimated cable. This is possibly due to the broader bandwidth of the 500 nm filters when the incident signal is at an angle from the normal, and suggests that the use of broader bandpass 500 nm filters would give higher signal levels with little or no increase in laser noise. The SMA terminated, uncollimated cable has a higher signal level than the line terminated cable, because more of the signal is directed onto the PMT head. Further optimization of the coupling of the fluorescent signal onto the PMT head could increase measured signal levels significantly.

The 442 nm filters can be expected to have no effect on signal level per mW of probe power, and a small effect on the noise level due to the low amount of power in the

wavelengths away from 442 nm. The 500 nm filters can be expected to have a large impact on both noise and signal levels. These effects are confirmed by the signal and noise data.

Examination of the signal levels measured for the bifurcated cables (figs 17-19) shows two distinct groups, with the combinations containing two 500 nm filters having lower signal levels than the combinations with only one 500 nm filter. The number of 442 nm filters has little effect. Data for the FFC (fig 16) is less conclusive, with the variability in the data due to inaccuracy in measuring the low signal levels involved.

Noise measurements (figs 12-15) show the same distinct groups, with the filter combinations with one 500 nm filter having higher noise than the combinations with two 500 nm filters, and only small reductions in noise levels within the groups as the number of 442 nm filters is increased. Variability of the data is more pronounced for noise measurements than for signal measurements in the bifurcated cables because the lower noise levels lead to greater inaccuracy in measurement. For the FFC, variability is actually reduced due to the relatively high noise level resulting from the direct noise path to the PMT.

The signal and noise data collected in the bench testing phase of this research have numerous sources of error. The oscilloscope used to measure PMT output had an inherent system noise that was typically on the order of 1-2 mV. The bleach effect has an impact on the measurements by making it difficult to accurately read the signal level before the signal decayed due to local heating of the oil. This error is difficult to estimate, but could be as high as 10% of measured signal levels. The power meter used to measure laser power is accurate to 0.02 mW, leading to some error in the reduction of data to a per mW basis. These errors in the data propagate through the calculated values of signal to noise ratio and figure of merit discussed below. When interpreting these results, it should be kept in mind that the bench test results are not precise, and are useful for general assessment of system configurations (e.g. choosing between fiber optic cables), but not for discerning small differences in performance between filter combinations with absolute certainty.

Signal to noise ratios (S/N) for the different combinations investigated were calculated. results can be found in figs 20-23. All values of S/N are on a per mW of probe power, per um of oil film thickness basis. Since signal increases with increasing oil film thickness and noise remains relatively constant, the S/N increases with increasing oil film thickness. As is expected, S/N increases with increased filtering, with the greatest improvement noted when the number of 500 nm filters is increased from one to two. The

significant scatter in the values of S/N, particularly in the case of the FFC, can be attributed to the propagation of error in the signal and noise measurements. Comparing overall S/N values for the different cables, one can rule out the FFC as a viable alternative to to its very poor S/N. Of the three bifurcated cables, the collimated bifurcated cable with SMA termination provides the highest values of S/N across all filter combinations.

In evaluating the best combination of filters and cable for use in the engine, three factors must be considered: S/N, signal level, and optimum probe power. S/N is important for good resolution, overall signal level per mW of probe power is important during fired conditions when the fluorescent signal decreases with the increased oil temperature, and the optimum probe power is important because it determines the absolute signal level. In order to evaluate the filter and cable combinations taking into account all three factors, a figure of merit (FOM) consisting of the product of S/N, probe power, and signal per mW per μm was calculated for each combination. Figs 24-26 show the FOM for each filter and bifurcated cable combination. The combination with the best FOM is the uncollimated SMA terminated bifurcated cable with two 500 nm filters and zero 442 nm filters.

An examination of Figs 24-26 illustrates the variability in the data collected for fluorescent signal and noise. The plots show a discernable trend, with FOM values being significantly decreased by increased 442 nm filtering, and slightly reduced by increased 500 nm filtering. The data does not, however, follow this trend precisely, substantial variation in measured values of FOM from the expected pattern are present. In particular, the best FOM for the bifurcated coaxial cable with a line end and the collimated bifurcated coaxial cable with an SMA end occur with filter combination 1 (zero 442 nm filters and one 500 nm filter), while the uncollimated bifurcated coaxial cable with SMA end has its best FOM with filter combination 4 (zero 442 nm filters and two 500 nm filters). This deviation in the expected pattern led to the conclusion that the scatter in the fluorescent signal and noise data resulted in FOM values that, while useful as rough gauges of performance between cables, are not sufficiently precise to make a judgement as to which filter combination is best for this application.

Test piece etch mark profiles obtained by both the profilometer and the laser fluorescence apparatus are shown in Fig 27. The area of interest for determining the resolution of the apparatus is the slope of the etch mark edge. The essentially equal slopes of the two traces in this area indicate that the profilometer stylus and the illuminated spot have the same resolution and hence roughly the same diameter. Since the stylus of the

profilometer has a diameter of 66 μm, this verifies that the illuminated spot produced by the focusing probe is indeed on the order of the expected size of 50 μm.

Based on the above analysis, it was decided to use the uncollimated, bifurcated cable with SMA termination in the engine test because of its high FOM for all filter combinations. It was further decided that all six filter combinations would be evaluated in the engine under motored conditions to determine the optimum choice, and to determine if the small variations in signal to noise observed in the bench tests between filter combinations were meaningful in the running engine.

8. ENGINE TESTING

In order to test the performance of the apparatus, data was collected from a Kubota EA300N single cylinder diesel engine. Specifications for this engine can be found in Fig 28. Data was collected under both motored and fired conditions at 1500 rpm using Pennzoil SAE 30 oil, standard Kubota top and second rings, and a low (4.6 lbf) radial tension two piece oil control ring. In order to establish a basis for comparison, oil sump temperatures and, in the case of fired tests, engine loads, were made to coincide with those under which data was collected by Bliven. Fig 29 shows the engine operating conditions for both current and Bliven data.

Prior to moving the apparatus to the cart as mentioned above, the output of the photomultiplier tube due to engine vibration was measured. Results are shown in Fig 30. This output level of the PMT would correspond to noise equal to about 0.5 to 1.0 μm in data from [1], using a pre-amplifier gain of 10**6 and a typical calibration coefficient of approximately 15 mV/μm.

Motored data was collected for each of the six filter combinations discussed in the bench test section in order to determine their relative performance in the running engine. The results were then evaluated, and only the optimum filtering was used in the fired trial.

The engine was flushed prior to the collection of data following the same procedure outlined in [1] to eliminate any traces of previous test oils and to remove carbon deposits in the engine. The piston was cleaned prior to engine assembly, with particular attention paid to the crown grooves. This cleaning results in a good outline of the crown grooves in the motored data, but the grooves foul after a short period of fired operation.

9. ANALYSIS OF ENGINE TESTING RESULTS

As mentioned earlier, the pre-amplifier used in this apparatus is not optimal for this application. In the engine testing portion of this research this defect is most apparent and most detrimental to the quality of the data collected. The quality of the engine test data suffers due to the relatively long time constant of the pre-amplifier, which tends to diminish horizontal resolution, causing a "smearing" of the film thickness trace, as well as preventing the output from reflecting the true magnitude of the fluorescent signal, causing the film thickness in certain portions of the trace to appear either too thin or too thick. Because of these deficiencies in the data it is not useful to make precise comparisons of data collected by this apparatus with those collected by previous researchers. By making qualitative comparisons, keeping in mind the limitations of the pre-amplifier, useful conclusions about the performance of this apparatus can be drawn, and the success of this research may be judged.

Film traces for the conventional optics system and the fiber optics system can be found in figs 31-34. These figures show overlays of 4 consecutive compression strokes. Data were calibrated using the dynamic calibration method discussed in [1]. The cutting off of the motored fiber optics film trace at 100 μm is due to the voltage limitation of the data acquisition system. Since the fiber optic system runs at an order of magnitude higher pre-amplifier gain than the conventional optics system, the voltage output levels of the fiber optics system are much greater than those of the conventional optics system. The regions of interest in the film trace (i.e. the ring contours, crown grooves, and etch marks) are still clearly visible. In the course of plotting this data, it was observed that the analysis program used for fluorescence data analysis, ANL, was not plotting the data correctly on the x-axis due to an incorrect value for the location of the BDC pulse. For the purpose of informing future researchers of this recurrent problem and to make suggestions for its permanent correction, notes are included in Appendix 2.

The resolution of the apparatus can be compared with the resolution of the conventional optics apparatus by examining the film traces in the region of the crown grooves. These grooves are uniform circumferentially and are stationary with respect to the piston, which makes comparison between data sets meaningful. Fig 35 shows the crown groove region for a fiber optics motored data set and Fig 36 shows the same region from the

conventional optics motored data set. An examination of the the two traces show that the film trace from the fiber optics apparatus is comparable to that obtained with the conventional optics system. Differences between the traces can be attributed to carbon deposits in the grooves that were not completely removed during the cleaning process. These results, in conjunction with the resolution measurement discussed in the bench test section, show that the horizontal resolution of the system is comparable to that of the conventional optics system.

Motored calibration coefficients for each filter combination are shown in Fig 37. Note that these data are not reduced to a per mW of probe power basis as were the bench test data. The general trend in calibration coefficients is what one would expect, with the calibration coefficients decreasing as the total number of filters is increased. The addition of 500 nm filters appears to affect the calibration coefficient about as much as the addition of 442 nm filters, the former due to attenuated signal and the latter due to reduced laser power at the oil film. The calibration coefficient obtained using conventional optics was 24.6 mV/um for similar engine operating conditions. Taking into account the difference in amplifier gain, the filter combination consisting of one 500 nm filter with no 442 nm filtering has a calibration coefficient of 15.5 mV/um.

The reduction in calibration coefficient between motored and fired data for the fiber optics and conventional optics systems is shown in Figs 38 and 39 respectively. A much greater reduction in calibration coefficient is observed in the case of the fiber optics system. This may be due to the very poor etch mark traces in the fiber optic data as compared to the conventional data, etch marks for conventional and fiber optics data are shown in Figs 40 and 41 respectively. The reason for this disparity in etch mark film trace quality is unknown, but this difference could cause a large error in the calibration of the data from the fiber optics apparatus.

In evaluating the effect of filtering on the signal to noise ratio of the system in the running engine, overlay plots of the top ring region were constructed for each of the filter combinations from the motored data. This region was chosen due to the high reflectivity of the piston ring face and the thin oil film under the ring. These plots can be seen in Figs 42-47. There is no apparent effect in increasing the filtering beyond one 500 nm filter prior to the PMT. The variation in oil film thickness from stroke to stroke is greater than any observable difference in reflected laser noise under the top ring. Based on this observation,

and to ensure a maximum calibration coefficient it was decided to use only one 500 nm filter and no 442 nm filtering in the fired engine test configuration.

To compare the signal to noise ratio of the apparatus with that of the conventional optics system, oil film traces in the top ring region of fired data sets were made for both systems. By fitting an appropriately scaled top ring contour to the plots, the resolution of the system under these conditions can be determined. Fig 48 shows a typical top ring contour fitted to an oil film trace taken from a conventional optics data set, Fig 49 shows the same ring fitted to a fiber optics film trace. In the conventional optics film trace, the limiting factor in fitting the ring contour is the apparently random noise on the order of 1 μm. This noise prevents the accurate determination of the oil film characteristics under the top ring. Important features to note in Fig 48 are the lump of oil preceding the ring, the lump of oil trailing the ring, and the plateau between these two features which indicates the position of the ring. An examination of Fig 49 shows the same features although somewhat diminished and distorted by the pre-amplifier. The absence of the random noise may be due to the difference in amplifier characteristics, or due to the isolation of the PMT from engine vibration in the fiber optics apparatus. Further evaluation of the apparatus with the correct pre-amplifier is required before a definitive judgement can be made.

10. CONCLUSIONS

The goals of this research were, as mentioned above: ease of installation, reduction in vibration effects, portability, and increased signal to noise ratio. In evaluating the design, it is relatively straightforward to judge its success in meeting the first three goals. Installation of the apparatus is much easier since the system requires essentially no optical alignment, vibration effects are eliminated by removing the laser and PMT from the engine test bed, and mounting the system on a wheeled cart makes the system portable. Assessing the system's performance in terms of an improved film trace quality requires a more careful analysis, even more so due to the use of a less than optimal pre-amplifier. A detailed discussion along these lines is contained in appendix 3. The system's performance, after careful assessment, can be said to be comparable to that of the conventional optics system.

REFERENCES

1.) Bliven, M. D., "Oil Film Measurements for Various Piston Ring Configurations in a Production Diesel Engine", S.M. Thesis, Massachusetts Institute of Technology, Department of Mechanical Engineering, June 1990.

2.) McElwee, M.R., "Comparison of Single-Grade and Multi-Grade Lubricants in a Production Diesel Engine", S.M. Thesis, Massachusetts Institute of Technology, Department of Mechanical Engineering, January 1990.

3.) Lux, J.P., "Lubricant Film Thickness Measurements in a Diesel Engine", S.M.Thesis, Massachusetts Institute of Technology, Department of Mechanical Engineering, May 1989.

4.) Parker, C.A., Photoluminescence of Solutions , Elsevier Publishing Company, 1968.

5.) Hoult, D.P., Billian, S.A., Lux, J. P., Wong, V. W., "Calibration of Laser Fluorescence Measurements of Lubricant Film Thicknesses in Engines", SAE Paper #881587, 1988.

5.) Hoult, D.P., Takaguchi, M., "Calibration of the Laser Fluorescence Technique Compared with Quantum Theory.", Sloan Automotive Laboratory, Massachusetts Institute of Technology, 1990.

APPENDIX 1: DESCRIPTION OF FIBER OPTIC CABLES

FUSED FIBER COUPLER (FFC)

The fused fiber coupler consists of a single 50 μm diameter fused silica fiber with three legs. The coupler is formed by laying two 50 μm fibers across each other, fusing the junction using an electric arc, and trimming off one of the four legs that result. The junction thus formed is not symmetric, and has different loss and transmission characteristics depending on which leg the light is traveling as it enters the junction. Fig 50 shows experimental results for junction loss and junction splitting for two fused fiber couplers. Each leg has an SMA termination which allows attachment to standard fiber optic components.

The flow path of laser light and fluorescent signal for the fused fiber coupler is shown in Fig 4. Laser light is focused into the fiber by the eccentric coupler after filtering as mentioned above. The laser light then travels down the fiber to the junction, where approximately 50% of the laser power is attenuated. The remaining laser light is then split between the two legs of the fiber in a roughly 98% to 2% ratio. The stronger leg transmits laser light to the oil film, while the weaker leg transmits a substantial amount of laser light directly to the PMT, where it becomes noise. This direct path noise can be minimized by judicious selection of the input and PMT legs of the fiber, but still is capable of saturating the photomultiplier tube unless filtered, being several orders of magnitude greater than the collected fluorescent signal.

The fluorescent signal is collected by the same fiber that transmitted the laser light to the oil film. The signal is transmitted to the junction where again the signal is attenuated by 50% and split in a rough 50% to 50% ratio. Thus, only 25% of the collected signal is carried to the PMT.

As can be seen from the above description, the presence of the junction in the fused fiber coupler causes three problems: attenuation of both laser power and signal power, loss of laser power and signal power by splitting, and direct path laser noise. To eliminate these problems, two solutions are possible. One possible solution is to filter the laser and fluorescence signals sufficiently to give an acceptable signal to noise ratio. This, however, also reduces the amount of fluorescence reaching the PMT by attenuating the incident laser power as well as the collected fluorescent signal transmitted to the PMT. The second, and more attractive, option was to develop an optical cable with separate illumination and signal

paths to eliminate junction losses and direct path noise. Coaxial bifurcated fiber bundles were developed to meet this need.

BIFURCATED COAXIAL CABLES

The first coaxial bifurcated fiber bundle developed had six collection fibers which were drawn out in a line at the PMT end. Since the PMT has a rectangular head, it was hoped that this arrangement would better utilize the PMT detection area and result in higher signal output. The emergence angle of the fiber,however, when taken into account with the space required between the fiber end and the PMT for optical filters results in the signal spreading beyond the dimensions of the PMT head, and thus a significant amount of signal is lost. The collection characteristics of this bundle were much improved over those of the fused fiber coupler, however, due to the 2300 % increase in collection fiber area.

In the second bundle developed, there are eighteen collection fibers, increasing the collection fiber area 7100 % over the fused fiber coupler and 200 % over the previous bifurcated bundle. The PMT end has a standard SMA termination. The SMA termination was used so that the signal could be collimated using a standard collimating probe, thus directing all of the signal onto the PMT head.

The flow paths of the laser and fluorescent signal through the coaxial bifurcated cables are shown in Fig 3. Laser light is filtered and coupled into the central 50 μm fiber as described previously. The laser light is transmitted directly to the oil film, and the resulting fluorescent signal is collected by the 100 μm diameter fibers located coaxially around the central fiber. This signal is then transmitted to the PMT.

The bifurcated coaxial fiber bundles eliminate the problems of junction attenuation, splitting, and direct path noise associated with the fused fiber coupler. In addition the greater number and diameter of collection fibers increases collected signal power.

APPENDIX 2: NOTES ON BOTTOM DEAD CENTER PULSE LOCATION AND ANL

In preparing this thesis, it was discovered that the analysis program used to plot the data obtained from the laser fluorescence technique (ANL) was incorrectly assigning a value of -180.0 degrees ATC as the location of the bottom dead center pulse, regardless of the actual value input in the program in the form of a series of if/then statements which assigned BDC pulse location on the basis of the date of the data set and the run number. This resulted in the data being plotted such that the piston rings appeared in a position that did not coincide with the actual location of the ring grooves on the piston. To correct this problem, the if/then statements were nullified using comment symbols, and the desired position for the BDC pulse input for each data set.

In plotting the data from ref [1], the BDC pulse was assigned the value determined by Bliven for this data, -180.926 degrees ATC. For the fiber optics data, BDC pulse location varied from the data in ref [1] due to the removal of the shaft encoder during the installation of the new radiator insert. Further difficulty was experienced in keeping the shaft encoder fixed to the shaft, resulting in variability of BDC pulse location between data sets. In order to determine the location of the BDC pulse for the motored fiber optics data, the position of the fourth crown groove was made to coincide with the 4 mm position on the piston when plotted with ANL, and thus reflect the true position of this groove on the piston. Since the crown grooves are not visible in the fired data, the trace was aligned such that the top ring region lay between 10 mm and 11mm. These adjustments were accomplished by adjusting the BDC pulse location input to the program, which was then recompiled and the data plotted.

Some variability is still evident in the axial positioning of the film trace between fiber optics data sets, and more significantly between the fiber optics data and the conventional optics data. While distortion of the trace in the regions of interest around the rings due to these discrepancies is negligible, steps need to be taken in order to ensure that future data is positioned correctly.

To correct this problem, two items must be addressed:

1.) The method of fixing the shaft encoder to the engine shaft must be improved and made more secure. Currently the encoder is held to the shaft with set

screws. At high rpm and/or under fired conditions these screws tend to loosen, at which point relative rotation occurs between the shaft encoder and the engine shaft and the BDC pulse location changes. A new coupler, preferably employing a key and keyway, would solve this problem.

2.) The location of the BDC pulse must be measured independent of the film trace. A more precise and repeatable method for measuring the location of the pulse in degrees ATC must be developed. Locating the position of the BDC pulse using the film trace itself is not precise enough to give accurate axial positioning of the film trace. Use of a dial indicator to precisely locate the position of the piston, in conjunction with an oscilloscope to read the BDC pulse, would enable the location of the BDC pulse to be measured precisely. This measurement would only need to be made once if the solid coupler mentioned above is used.

APPENDIX 3: EVALUATION OF SYSTEM COMPONENTS AND SUGGESTIONS FOR FUTURE RESEARCH

The laser, PMT, and data acquisition system components of this design are identical to those used by Bliven, and therefore do not contribute to any change in film trace quality between the two systems. The important components to examine are the laser coupler, the fiber optic cable,the focusing probe, the coupling of the fiber optic cable to the PMT and the geometry of the cable end termination, the narrow band filters used, the engine fixturing, and the PMT pre-amplifier.

The laser coupler is the best commercially available method. The low coupling efficiency is a major drawback as it partially negates the gains made by eliminating the optical train and its attendant inefficiency. Efforts should be made to improve this coupling efficiency as any increase in laser power on target would increase the fluorescent signal produced .

The bifurcated coaxial SMA terminated cable appears to be a good choice for this application. The large number of collection fibers collect an adequate signal, and the small diameter illumination fiber gives a small enough spot size for good resolution. Any further increase in the number of collection fibers would not give any improvement in signal, merely increase its magnitude. Any further decrease in the diameter of the illumination fiber would improve the resolution of the system, but at the cost of a further degradation of laser power incident on the oil film due to a lower laser coupling efficiency

The focusing probe performs well in terms of magnification and focal length. If the size of the probe could be reduced, the system could be made much more flexible in terms of possible probe positions within the engine. Efforts should be directed at developing a smaller probe.

The coupling of the fiber optic cable to the PMT requires further optimization. The emergence angle of the collection fibers needs to be considered in the design of a coupling fixture that maximizes fluorescent signal incident on the PMT head, while not locally saturating the PMT. The line termination may be reconsidered for use on a bifurcated cable with eighteen collection fibers rather than six collection fibers, and its performance reevaluated.

A wider bandpass 500 nm filter should be evaluated for use in the system. The characteristics of the noise and fluorescent signal spectra are such that a 20 nm or perhaps wider bandwidth would greatly increase detected fluorescent signal with a negligible increase in noise.

The engine fixturing design was driven largely by the size of the focusing probe. Again, if the probe size could be reduced, the size of the fixturing could be reduced, and the system made more flexible in its application. The improved o-ring seal should be retained in any future design requiring watertightness as it is a vast improvement over the previous seal.

As discussed at length in previous sections of this paper, the pre-amplifier used in the system is wholly inadequate for the acquisition of analysis quality data. The repair and implementation of the pre-amplifier used in previous research should be the number one priority of future researchers.

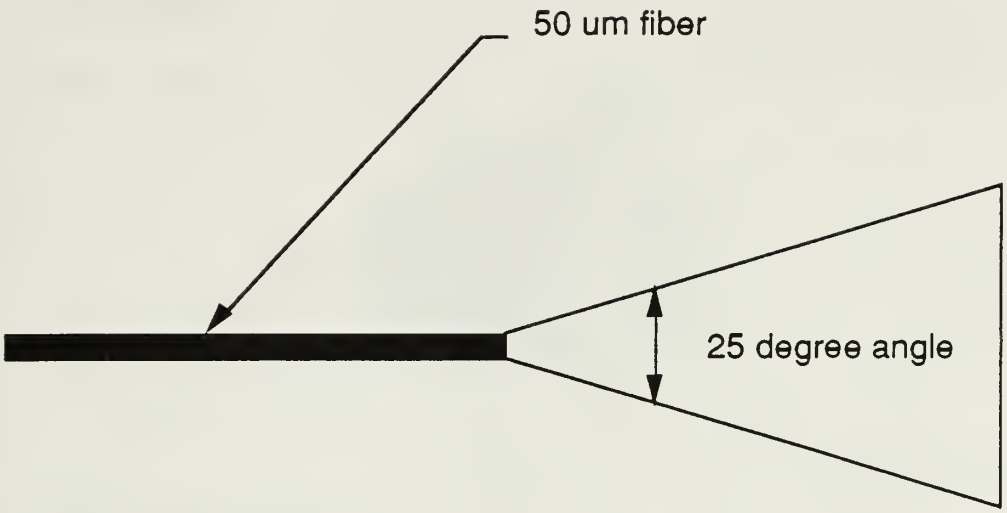

DISTANCE FROM END (um)	SPOT SIZE
10	54.4
20	58.9
30	63.3
40	67.7
50	72.2
60	76.6
70	81.0
80	85.5
90	89.9
100	94.3
113	100.0
150	116.5
200	138.7

Figure 1: Emergence angle and its effect on illumination spot size as distance from fiber is increased.

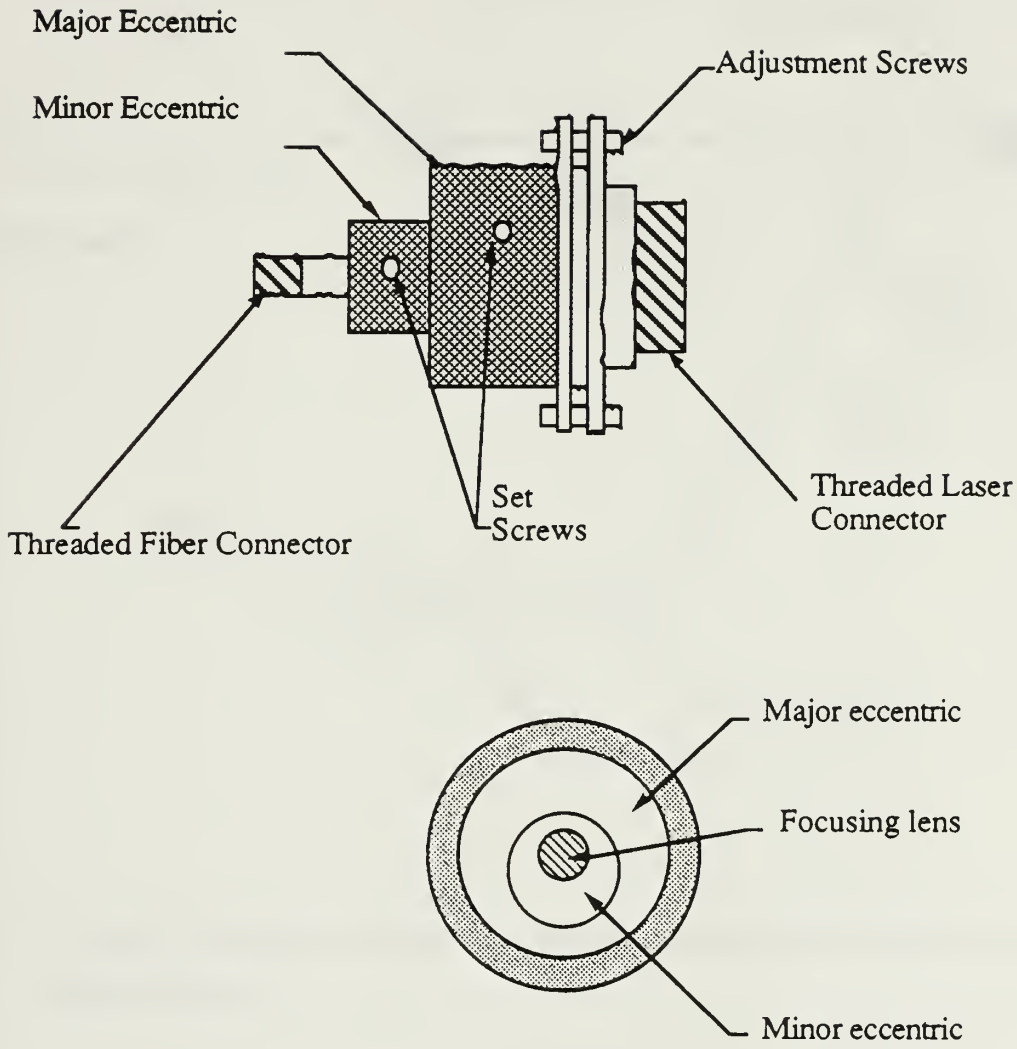

Fig 2: Eccentric coupler for coupling laser beam into illumination fiber.

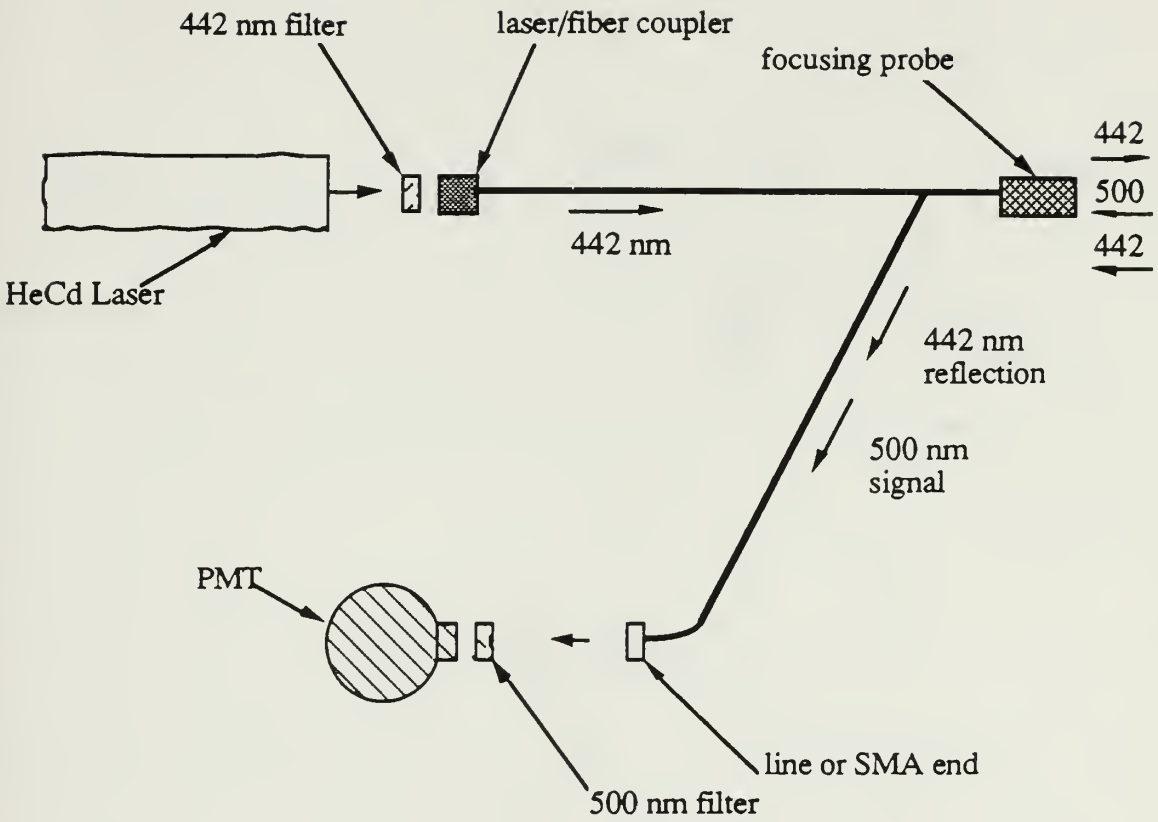

Figure 3: Diagram of bifurcated coaxial cable system showing flow paths of laser noise and fluorescent signal.

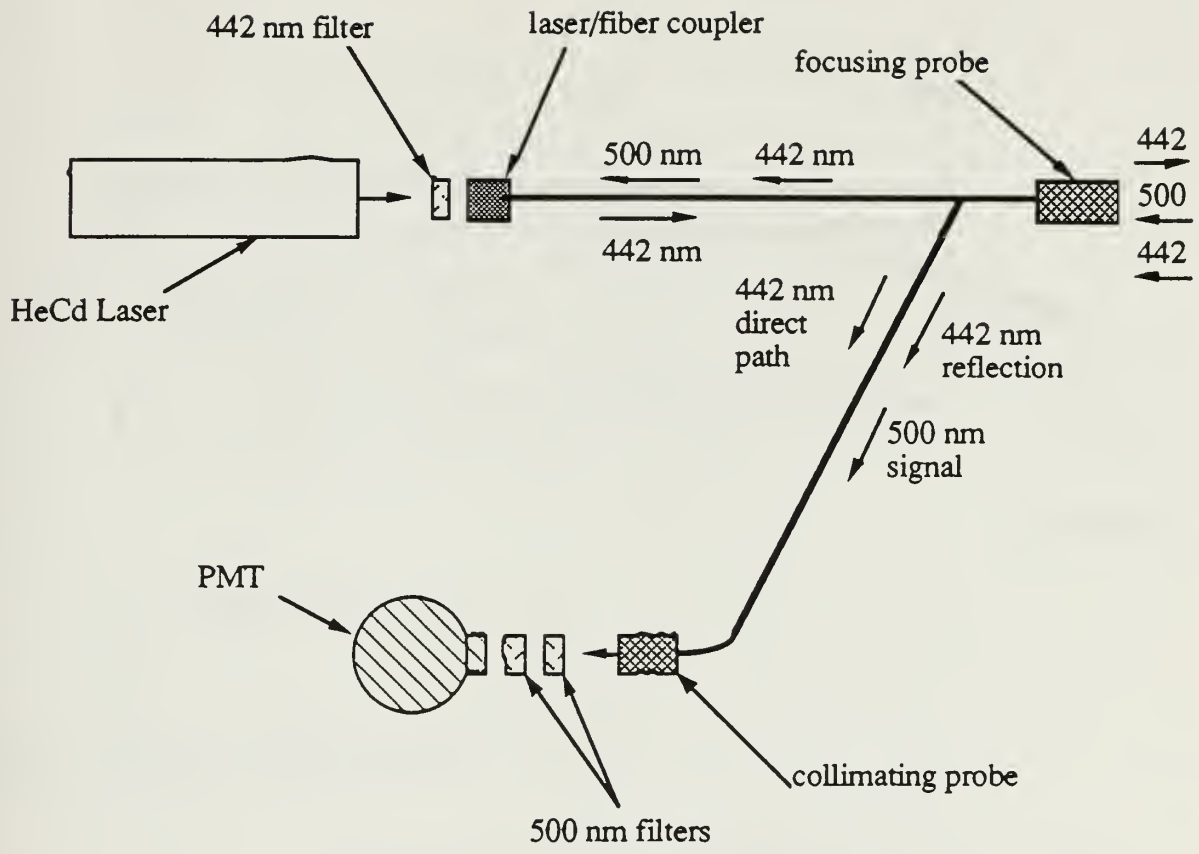

Figure 4: Diagram of fused fiber coupler system showing flow paths of laser noise and fluorescent signal.

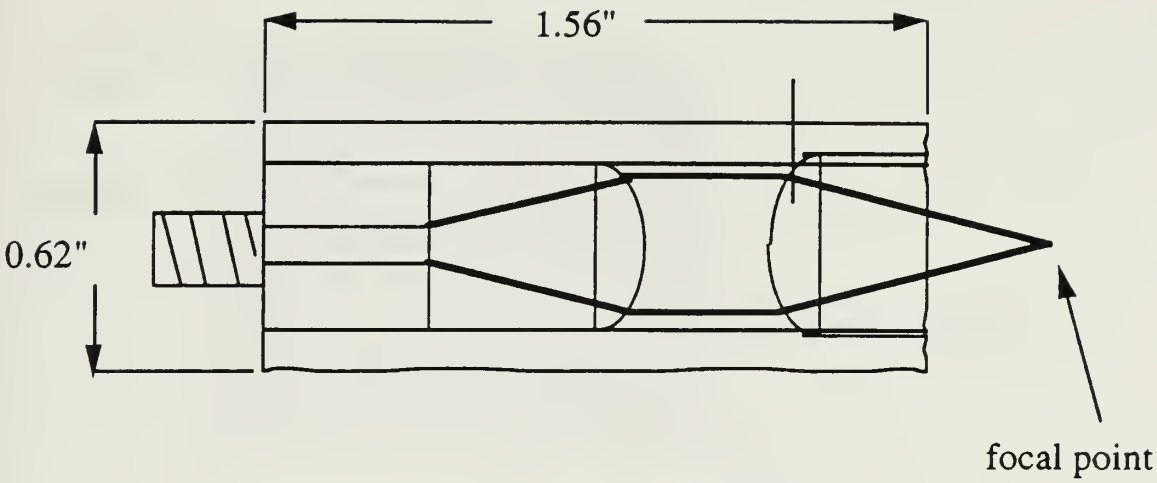

magnification = 1:1

Figure 5: Diagram of focusing probe.

	442 nm filter	500 nm filter
center λ (nm)	442 nm	500 nm
bandwidth (nm)	10 nm	10 nm
rejection outside band	10**-5 , 10**-6	10**-5 , 10**-6
transmission at center λ (%)	71%	69%

Figure 6: Specifications for 500 nm and 442 nm narrow band filters.

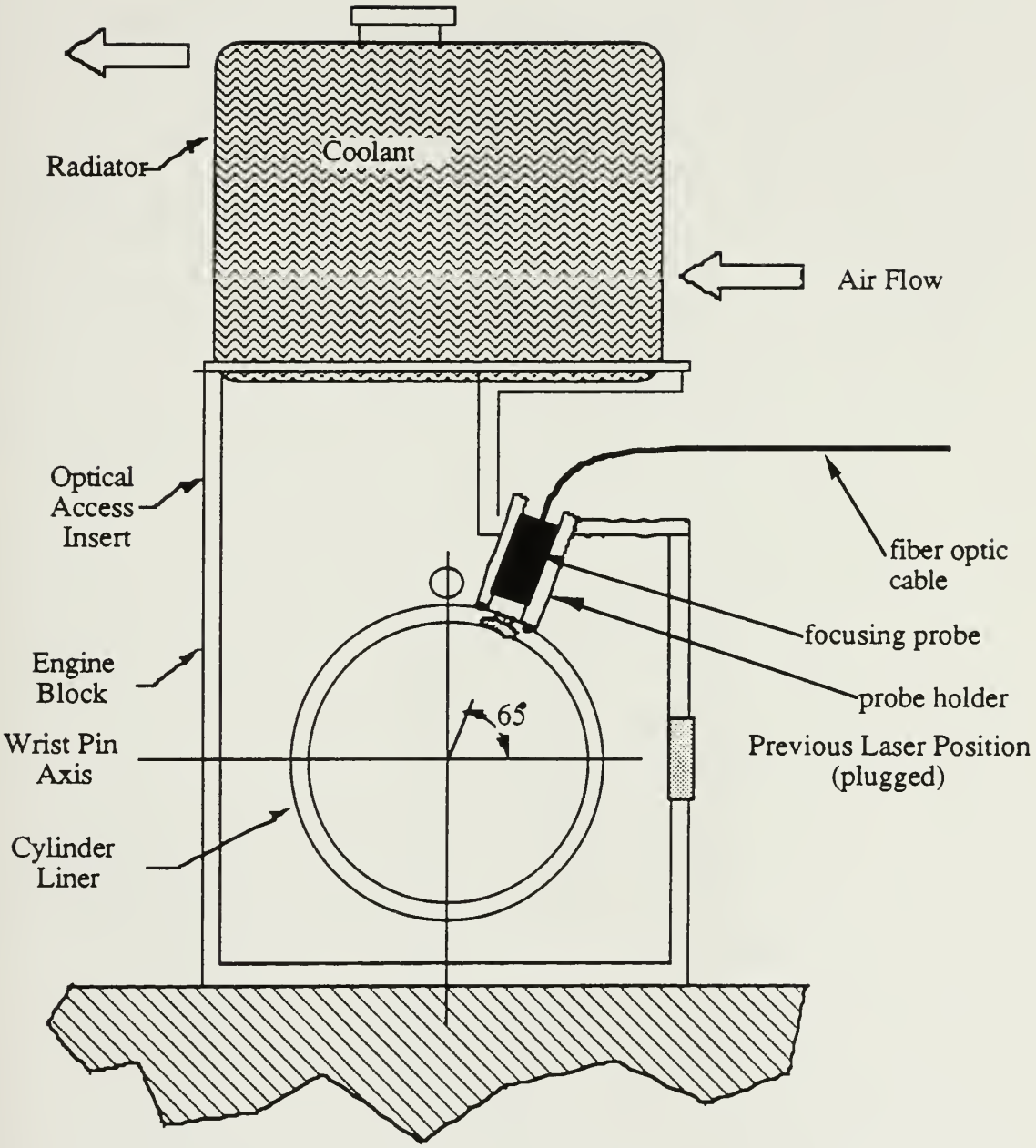

Figure 7: Modified engine.

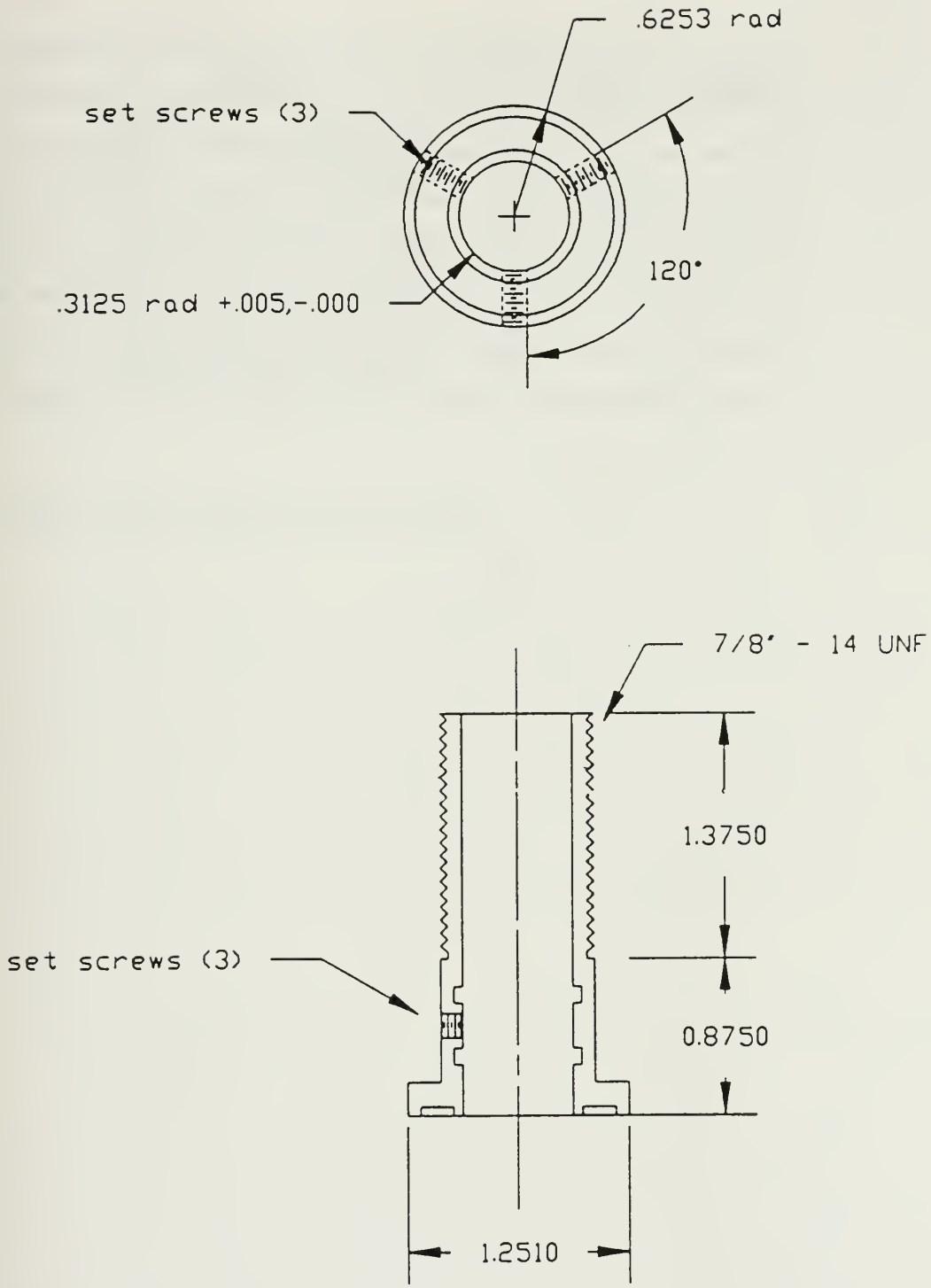

Figure 8: Focusing probe holder. All dimensions in inches.

FILTERS	COMBO NUMBER
ZERO 442 nm, ONE 500 nm	1
ONE 442 nm, ONE 500 nm	2
TWO 442 nm, ONE 500 nm	3
ZERO 442 nm, TWO 500 nm	4
ONE 442 nm, TWO 500 nm	5
TWO 442 nm, TWO 500 nm	6

Figure 9: Filter combination nomenclature.

	FILTER COMBINATION					
NOISE TEST	1	2	3	4	5	6
Pa (mW)	17	17	17	17	17	17
Pp (mW)	3.4	3	2.2	3.8	3.2	2.4
Psma (mW)	5	4	3	5.2	4	3
fl (in)	.1515	.1515	.1515	.1515	.1515	.1515
Nsma (mV)	0	0	0	0	0	0
Np (mV)	0	0	0	0	0	0
Ndry (mV)	1.5	1	1	1	1	.5

SIGNAL TEST	1	2	3	4	5	6
Pa (mW)	17	17	17	16	16	16
Pp (mW)	7.2	5.7	4	6	4.6	3.6
SIGNAL (mV)	150	120	80	110	76	56
SIGNAL (mV)	130	128	80	128	68	56
SIGNAL (mV)	150	112	80	92	68	56
SIGNAL (mV)	145	140	72	112	80	56
SIGNAL (mV)	150	110	96	120	88	56

Figure 10: Bench testing matrix. Data shown is for bifurcated coaxial cable without collimation.

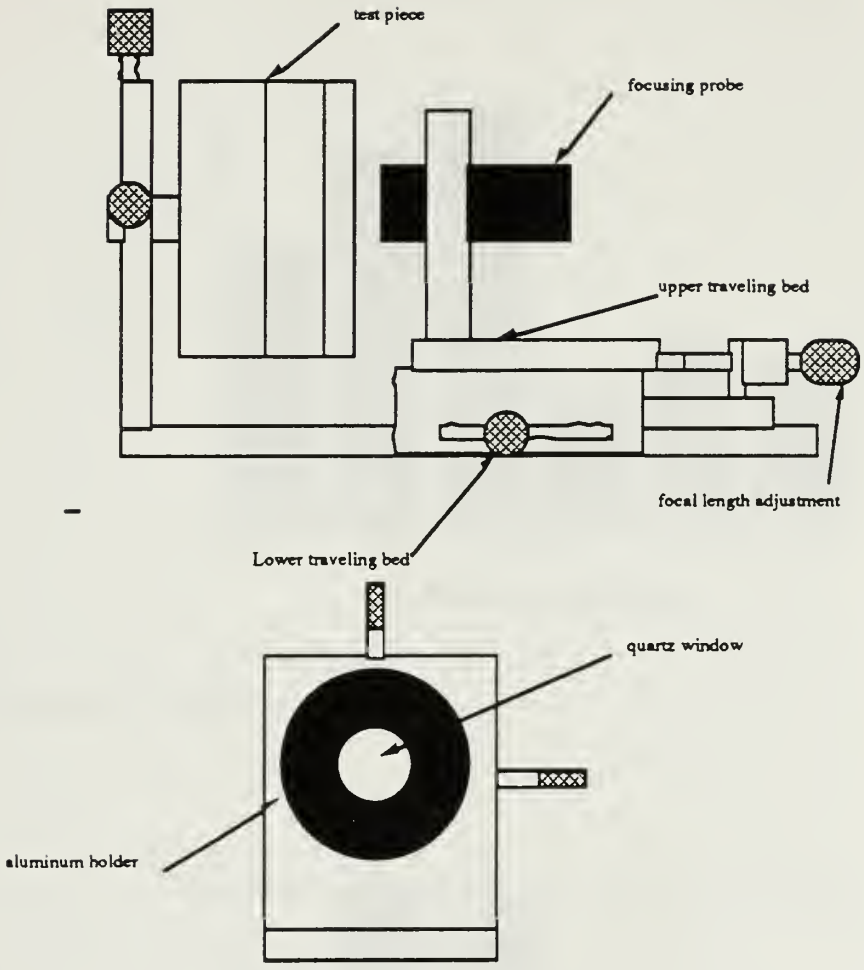

Fig 11: Bench testing apparatus.

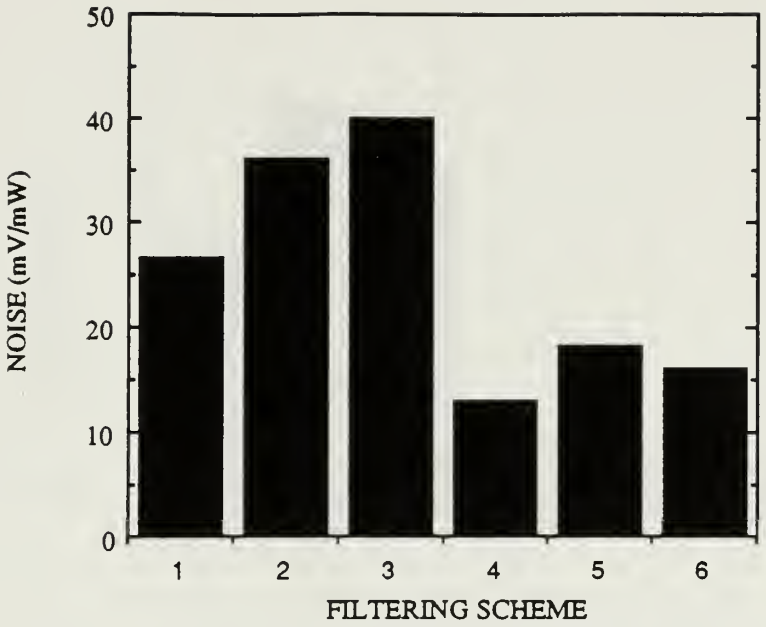

Figure 12: Noise vs filter combination for FFC.

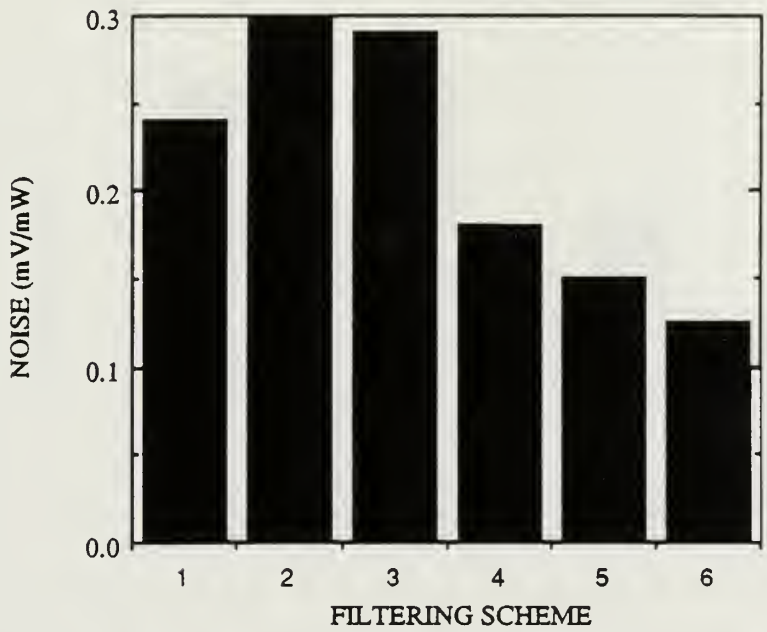

Fig 13: Noise vs filter combination for bifurcated coaxial bundle with line end.

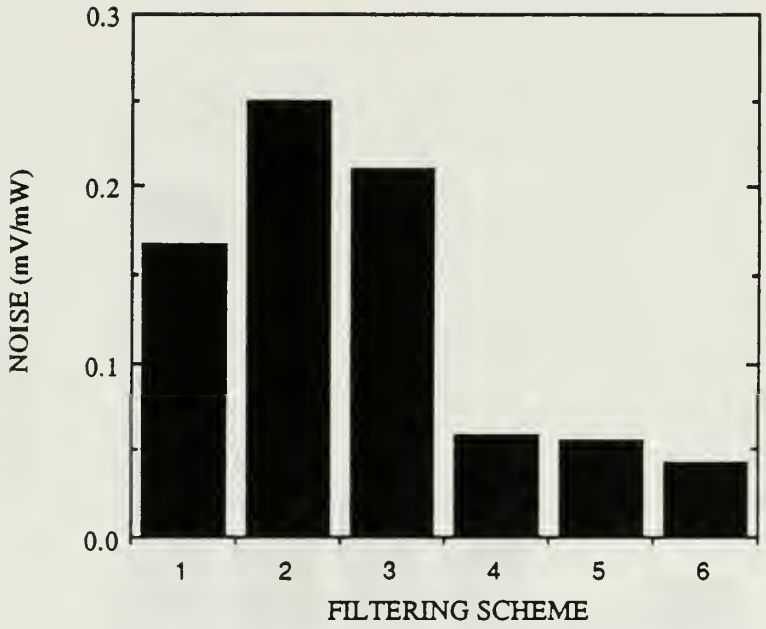

Fig 14: Noise vs filter combination for bifurcated coaxial cable with SMA end (collimated).

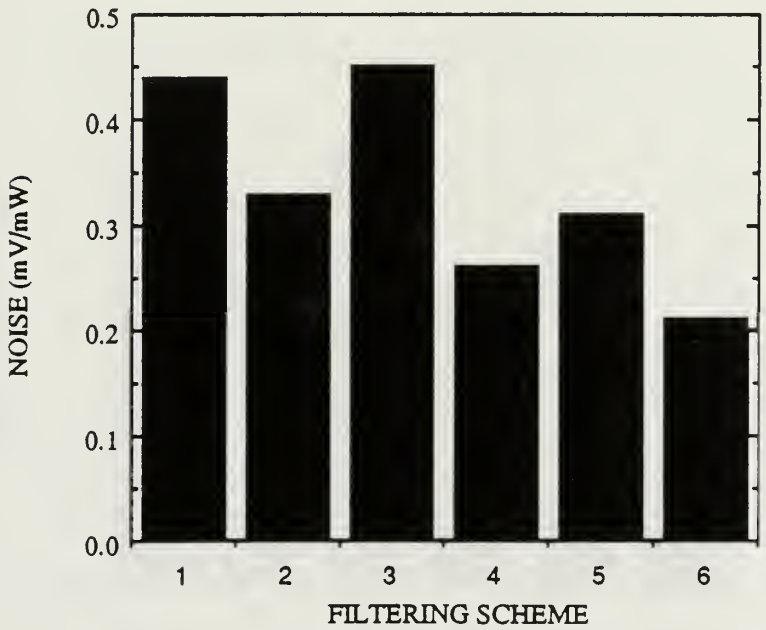

Fig 15: Noise vs filter combination for bifurcated coaxial cable with SMA end (uncollimated).

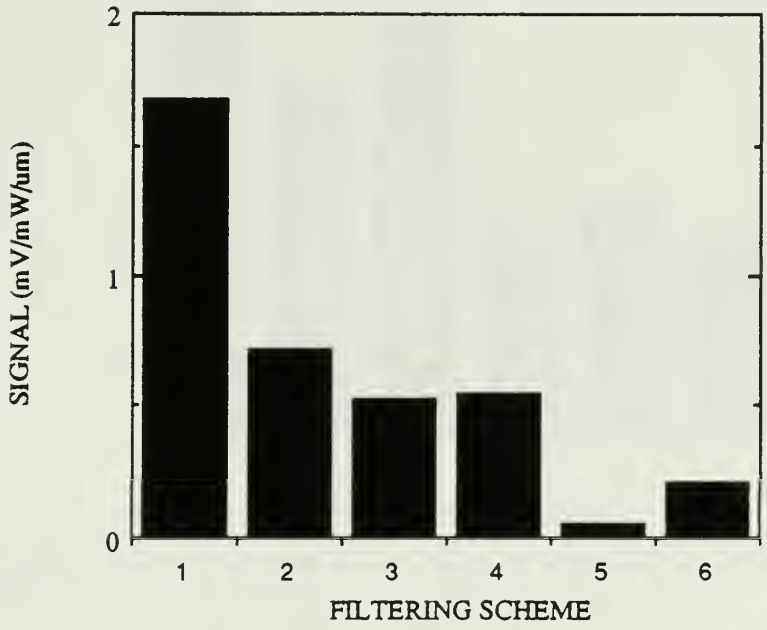

Fig 16: Fluorescent signal vs filter combination for FFC.

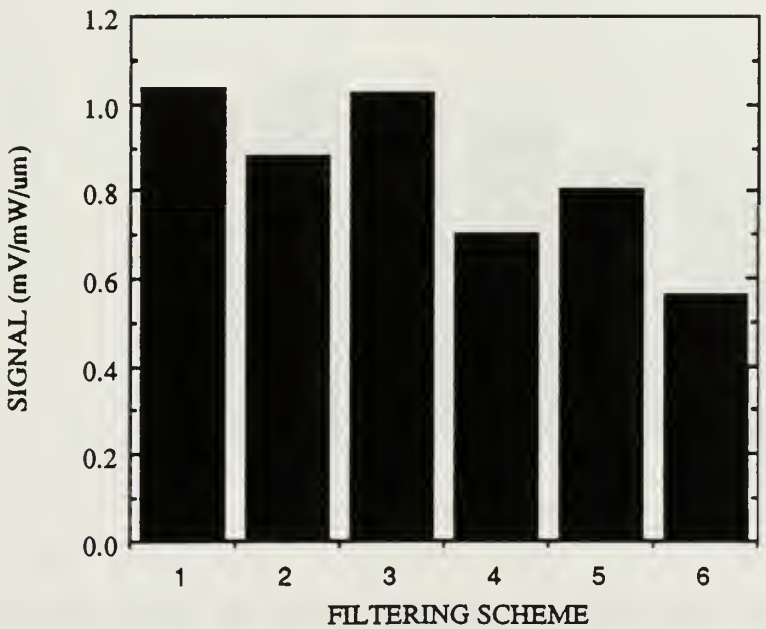

Fig 17: Fluorescent signal vs filter combination for bifurcated coaxial cable with line end.

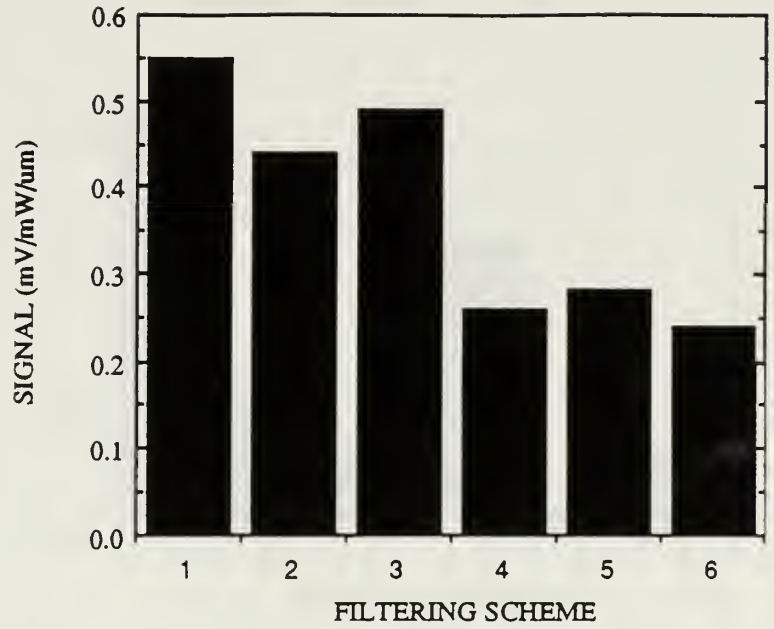

Fig 18: Fluorescent signal vs filter combination for bifurcated coaxial bundle with SMA end (collimated).

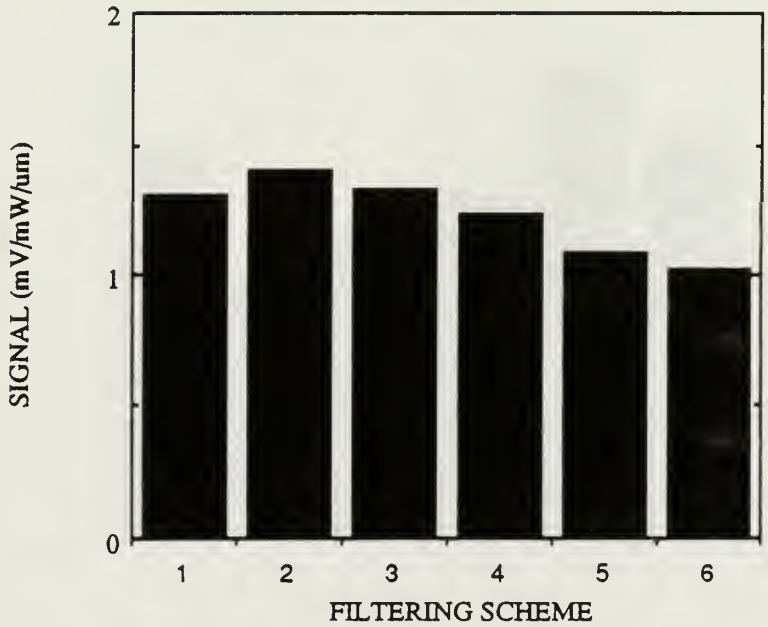

Fig 19: Fluorescent signal vs filter combination for bifurcated coaxial cable with SMA end (uncollimated).

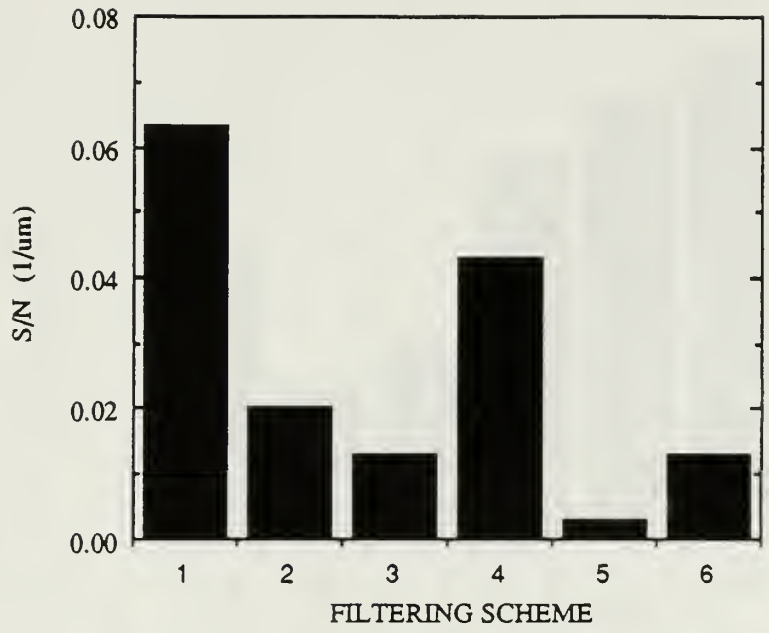

Fig 20: Signal to noise ratio vs filter combination for FFC.

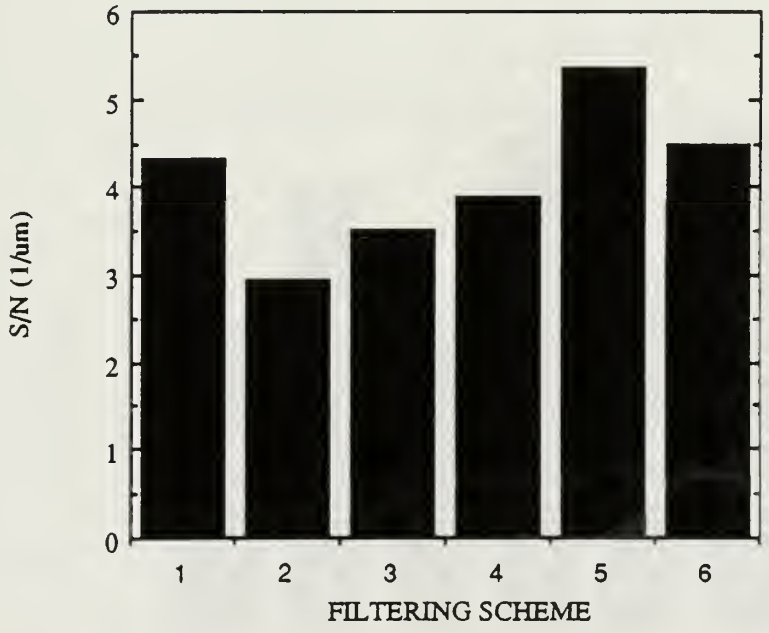

Fig 21: Signal to noise ratio vs filter combination for bifurcated coaxial cable with line end.

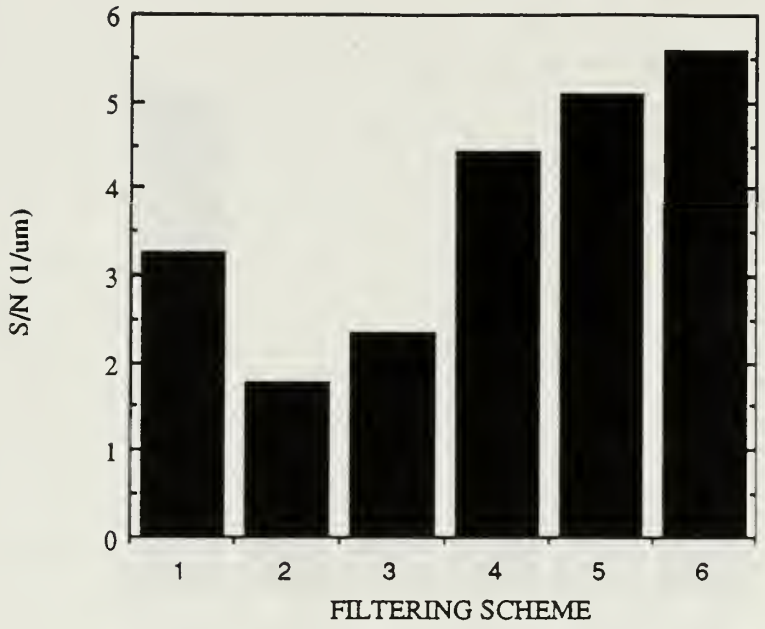

Fig 22: Signal to noise ratio vs filtering combination for bifurcated coaxial cable with SMA end (collimated).

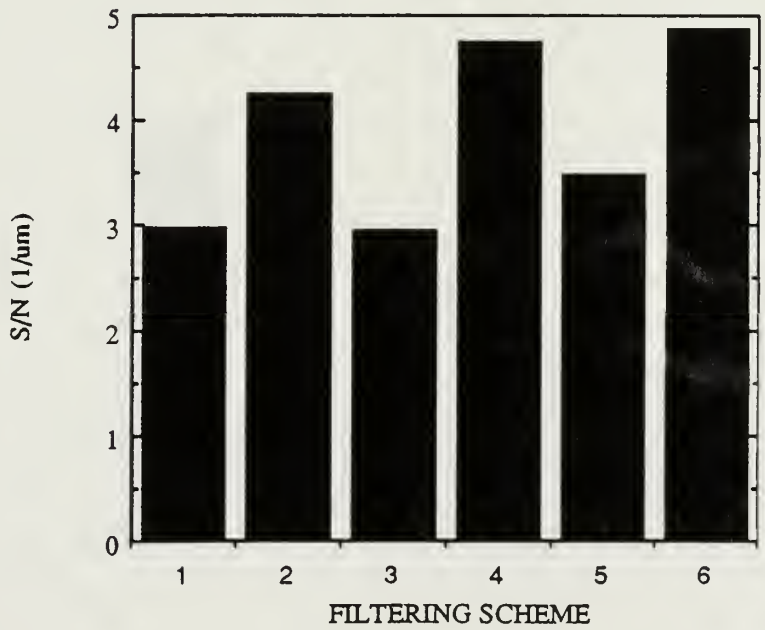

Fig 23: Signal to noise ratio vs filter combination for bifurcated coaxial cable with SMA end (uncollimated).

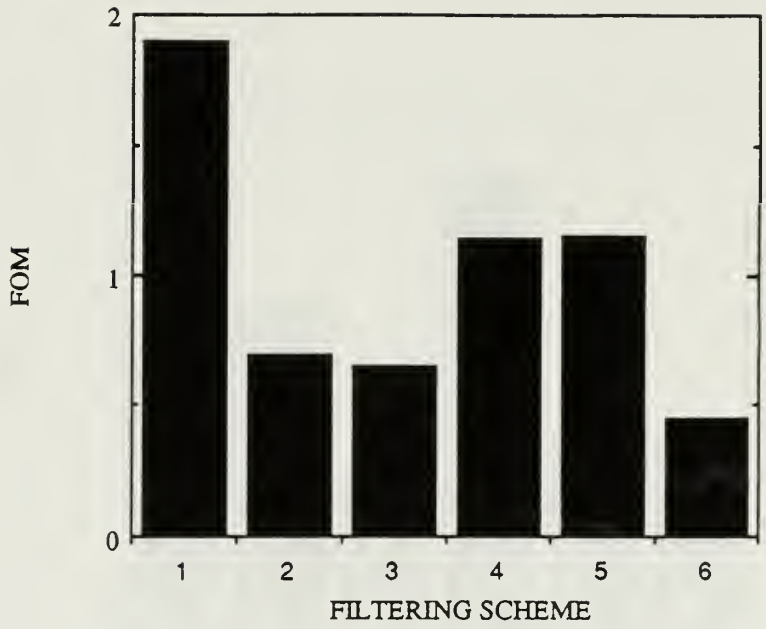

Fig 24: Figure of Merit (FOM) for each filter combination for bifurcated coaxial cable with line end.

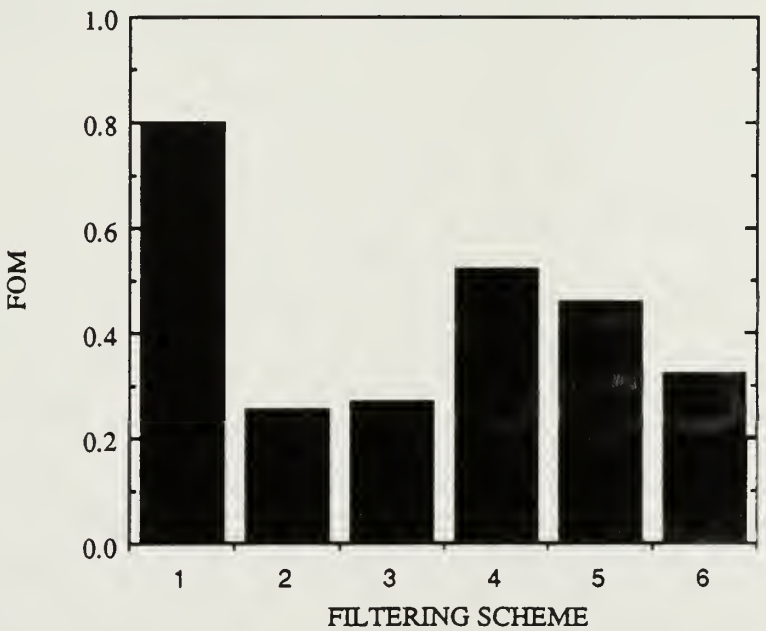

Figure 25: Figure of Merit (FOM) for each filter combination for bifurcated coaxial cable with SMA end (collimated).

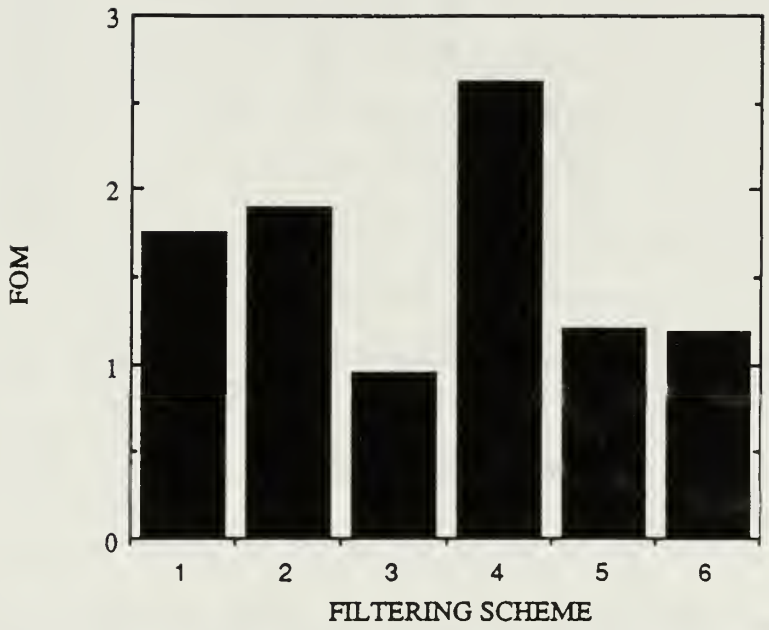

Figure 26: Figure of Merit (FOM) for each filter combination for bifurcated coaxial cable with SMA end (uncollimated).

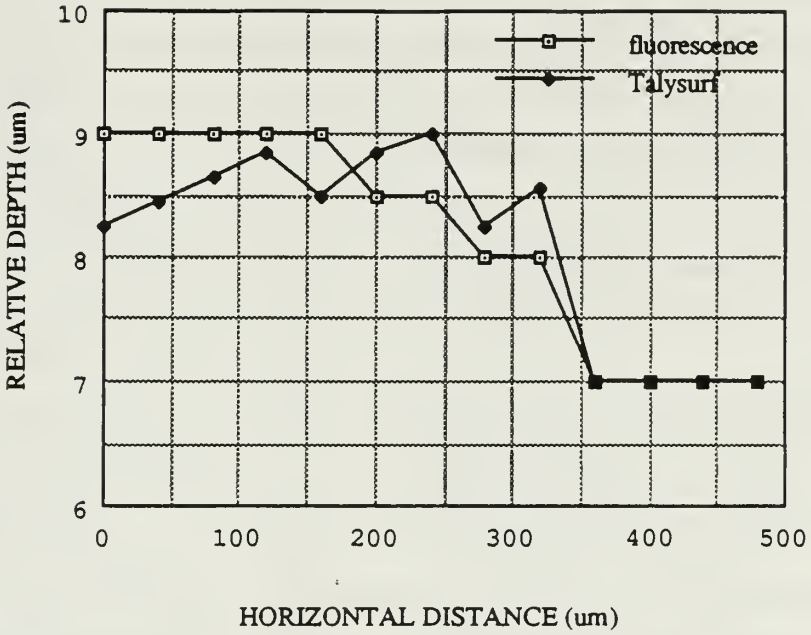

Fig 27: Plot showing resolution of combination of 50 μm illumination fiber and focusing probe.

MAKE	KUBOTA
MODEL	EA 300N
TYPE	Horizontal, 4 stroke, IDI diesel
NO. CYLINDERS	1
BORE AND STROKE	75 x 70 mm (2.95 x 2.76 in)
DISPLACEMENT	0.309 l (18.86 cu. in.)
COMPRESSION RATIO	23:1
COOLING SYSTEM	Water cooled/ Natural convection
LUBRICATION SYSTEM	Trochoidal pump/ no oil filter
RATED BHP	4.48 kW @ 3000 rpm (6 bhp)
MAXIMUM TORQUE	15.2 Nm (11.2 ft-lbf)
TYPICAL APPLICATION	Remote power generation

Figure 28: Specifications for test engine, from [1].

PARAMETER	CONVENTIONAL OPTICS		FIBER OPTICS	
	MOTORED	FIRED	MOTORED	FIRED
OIL TEMP (F)	117	164	118	178
COOLANT TEMP (F)	115	163	92	133
EXHAUST TEMP (F)	84	767	82	809
LOAD (LBF)	N/A	+8.0	N/A	+7.6
ATM P (mm Hg)	766.2	766.2	736.6	752.8
REL HUM (%)	59.5	59.5	68	71
INTAKE PRESS (in H2O)	1.61	1.11	1.9	2.0
INTAKE TEMP (C)	26	28	25	27

Figure 29: Engine operating conditions.

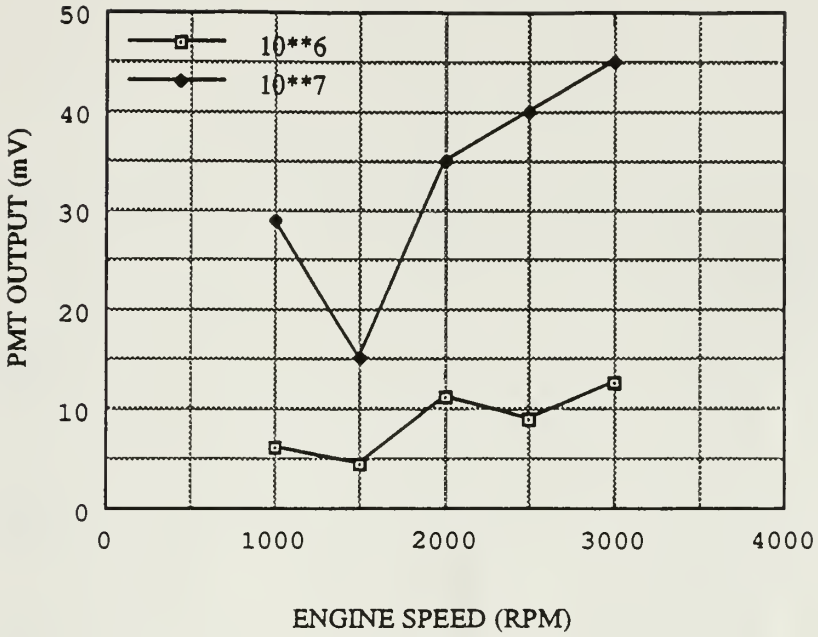

Fig 30: Vibration noise in PMT vs engine speed for PMT pre-amplifier gains of 10**6 and 10**7.

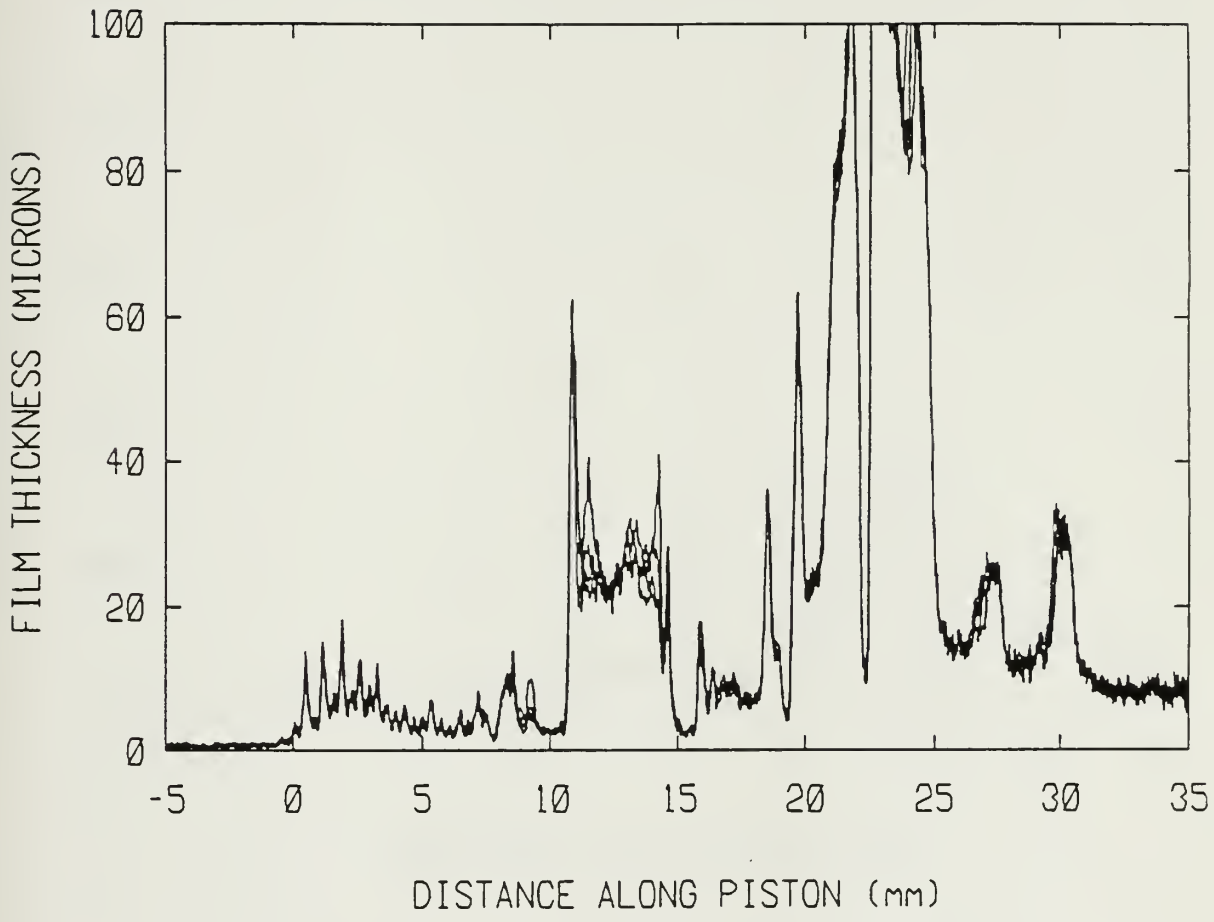

Figure 31: Motored film trace from conventional optics data. Trace represents overlay of 4 consecutive compression strokes, direction of piston travel is right to left.

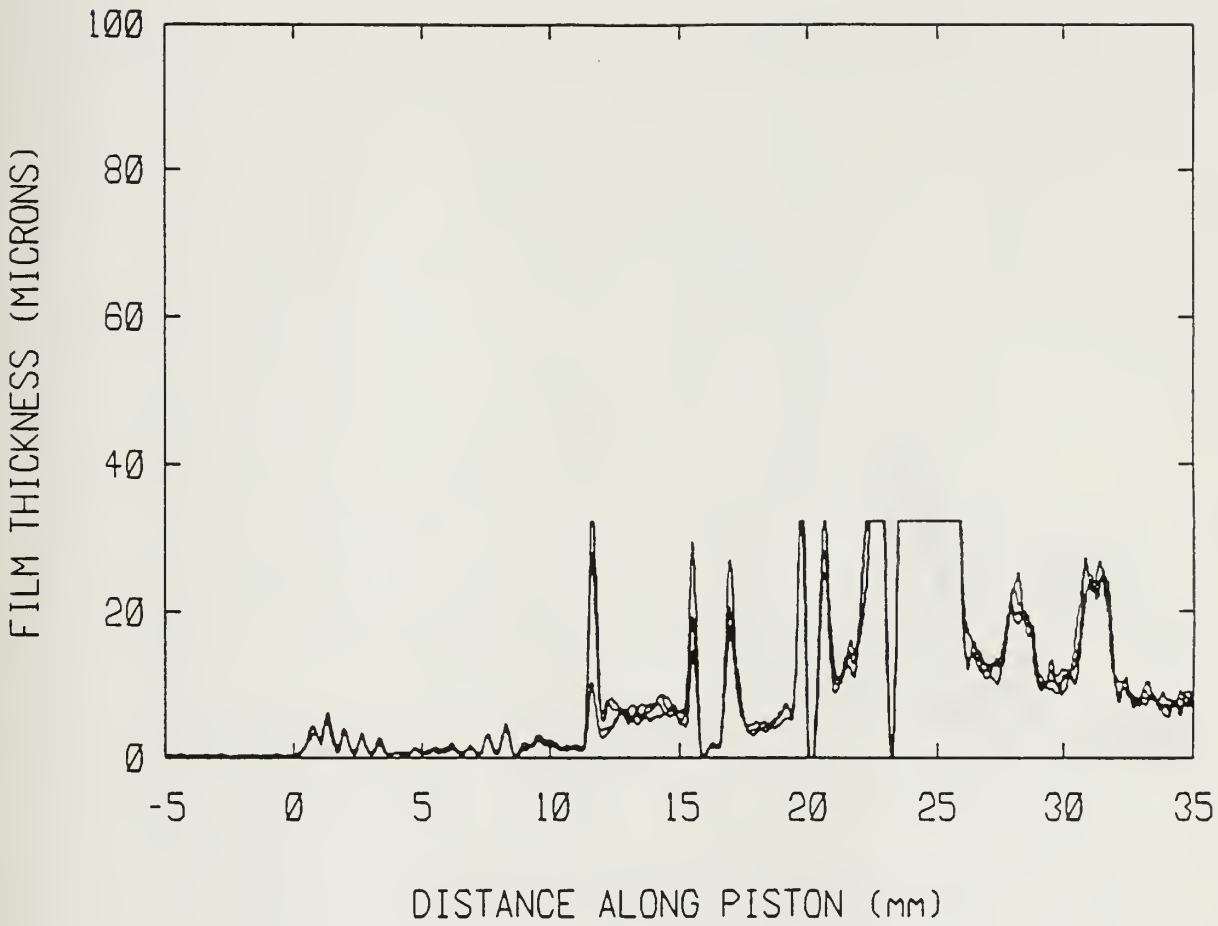

Figure 32: Motored film trace from fiber optics data. Trace represents overlay of 4 consecutive compression strokes, direction of piston travel is right to left.

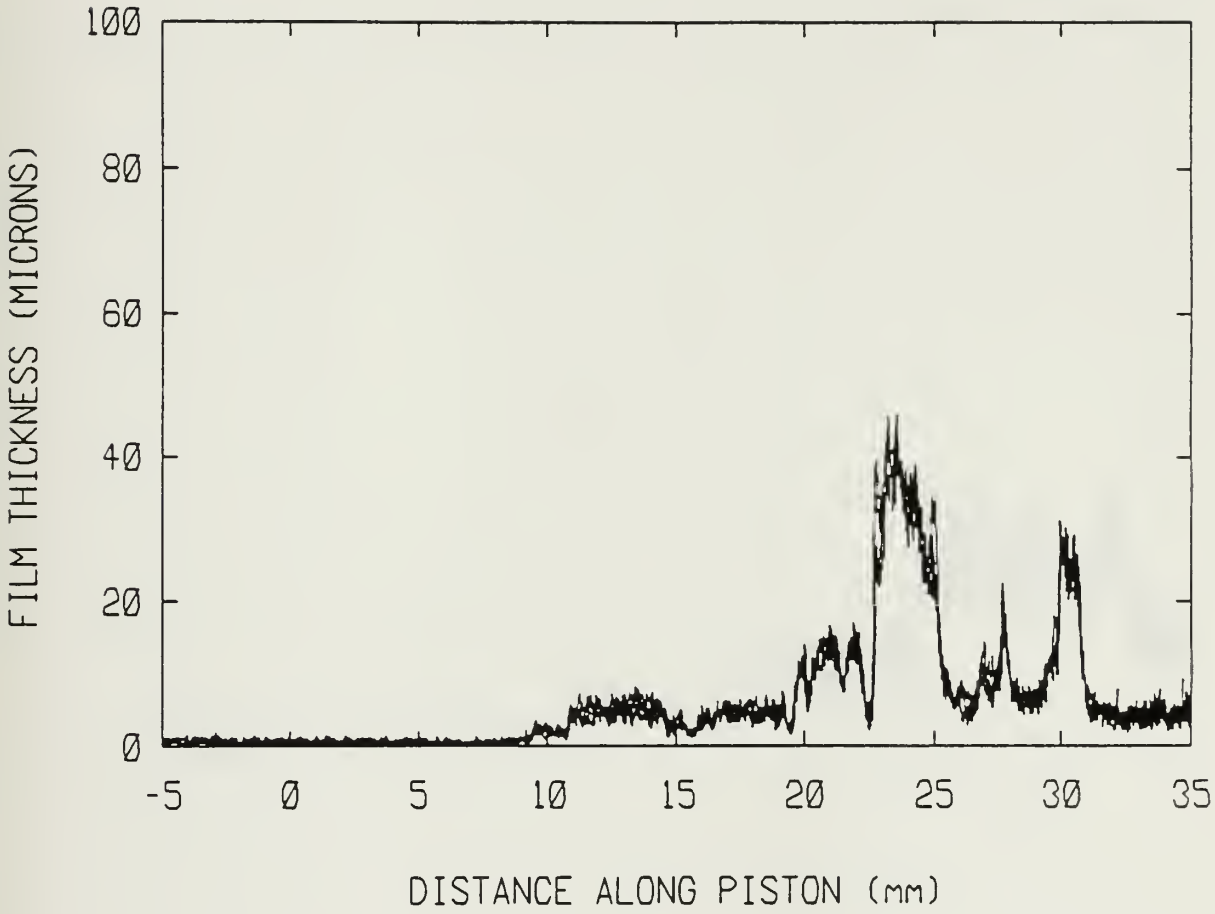

Figure 33: Fired film trace from conventional optics data. Trace represents overlay of 4 consecutive compression strokes, direction of piston travel is right to left.

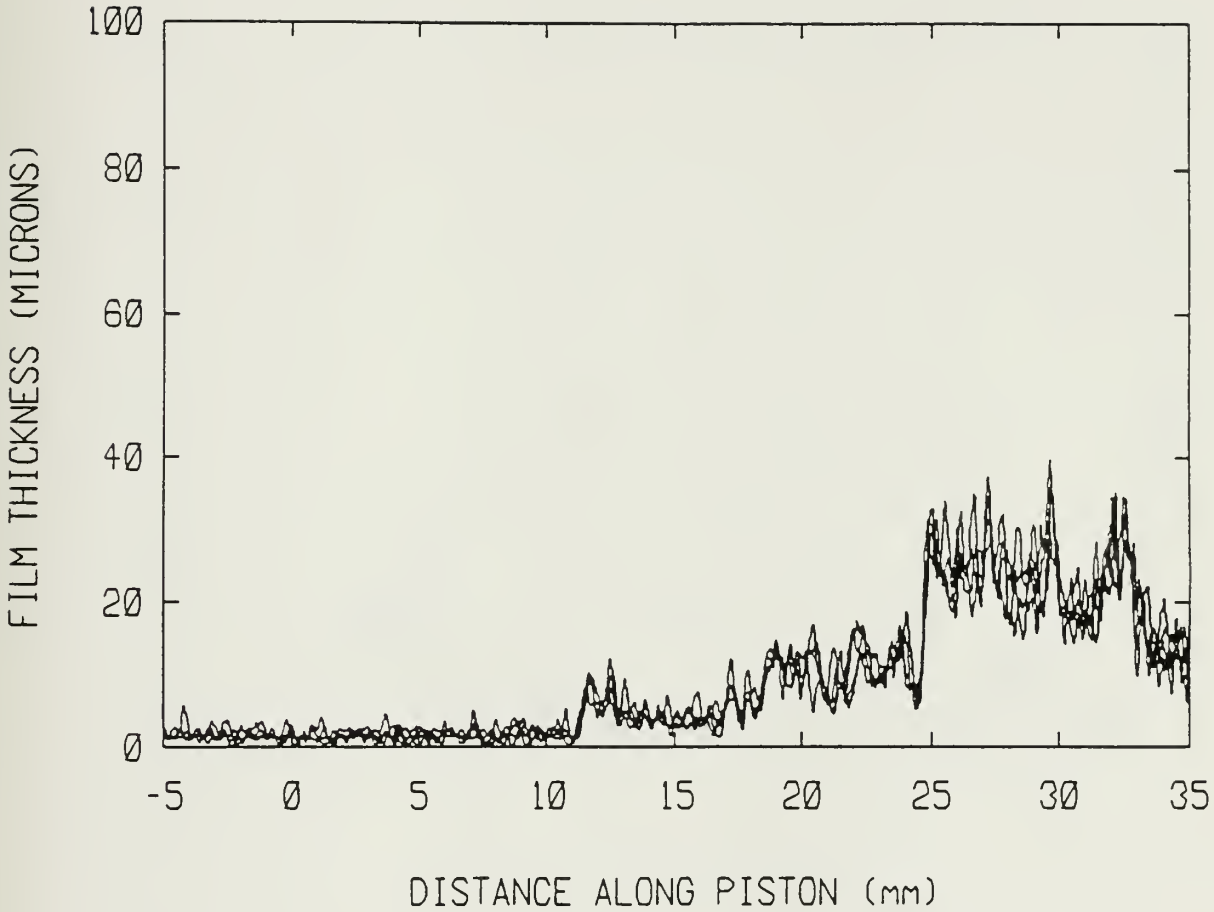

Figure 34: Fired film trace from fiber optics data. Trace represents overlay of 4 consecutive compression strokes, direction of piston travel is right to left.

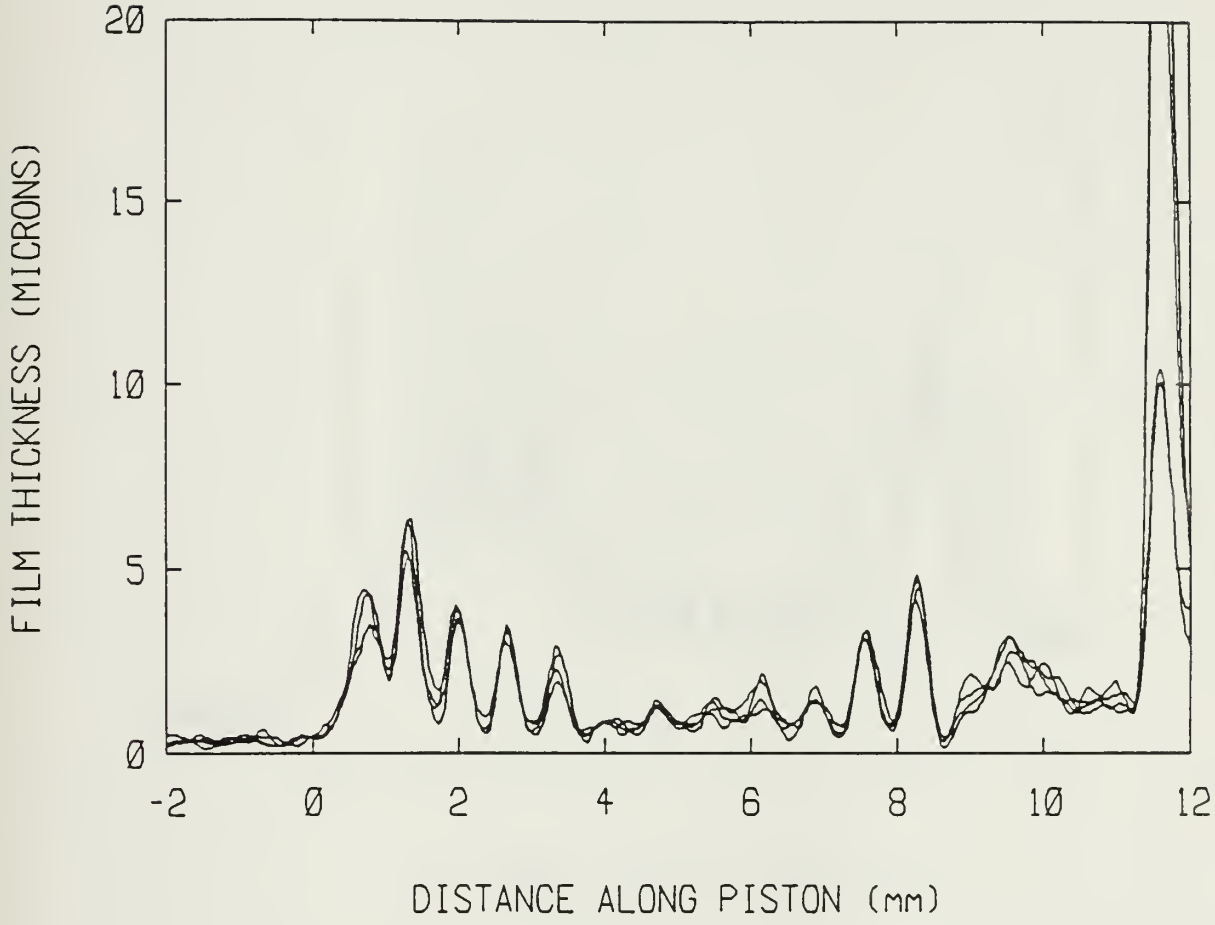

Figure 35: Detail of motored film trace in crown groove region from fiber optics data. Trace represents an overlay of 4 consecutive compression strokes, direction of piston travel is right to left.

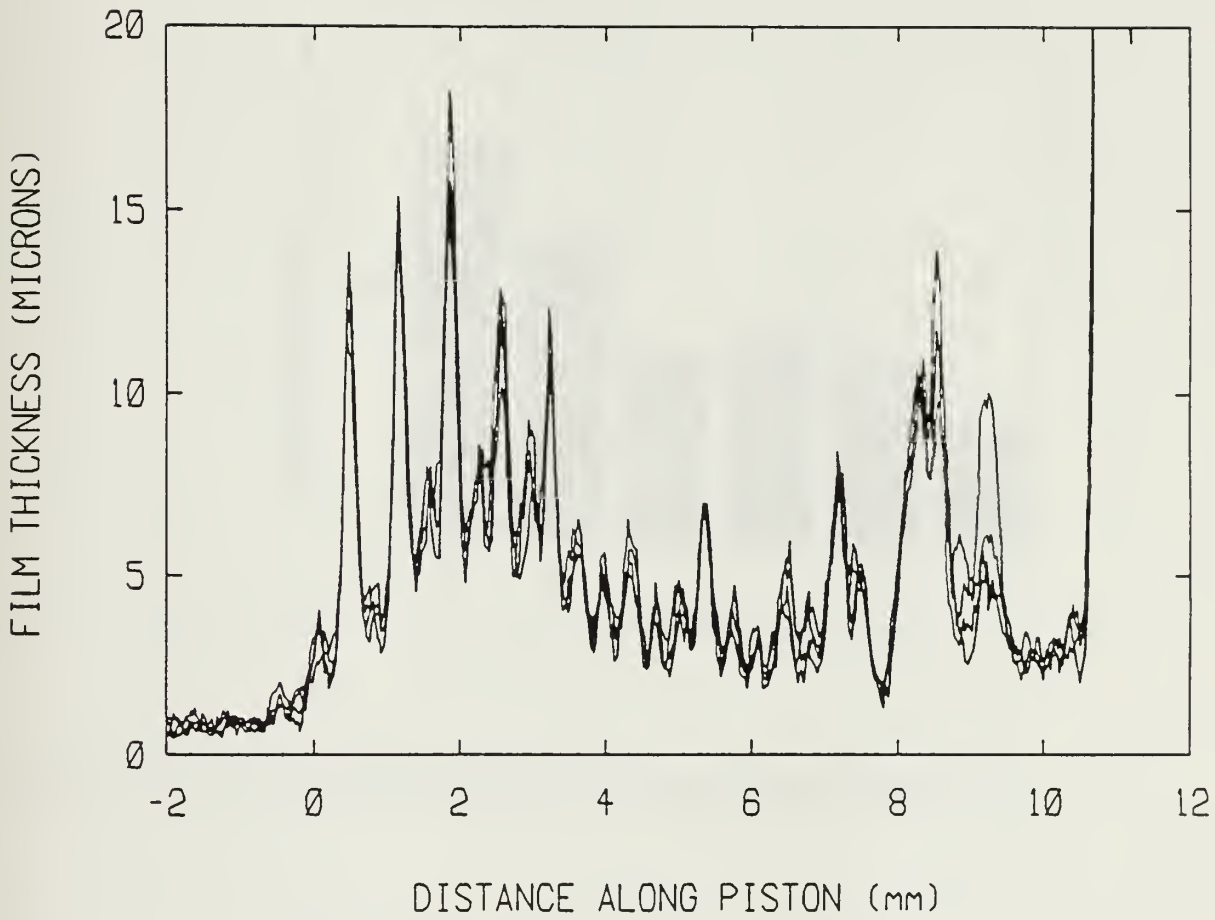

Figure 36: Detail of motored film trace in crown groove region from conventional optics data.Trace represents an overlay of 4 consecutive compression strokes, direction of piston travel is right to left.

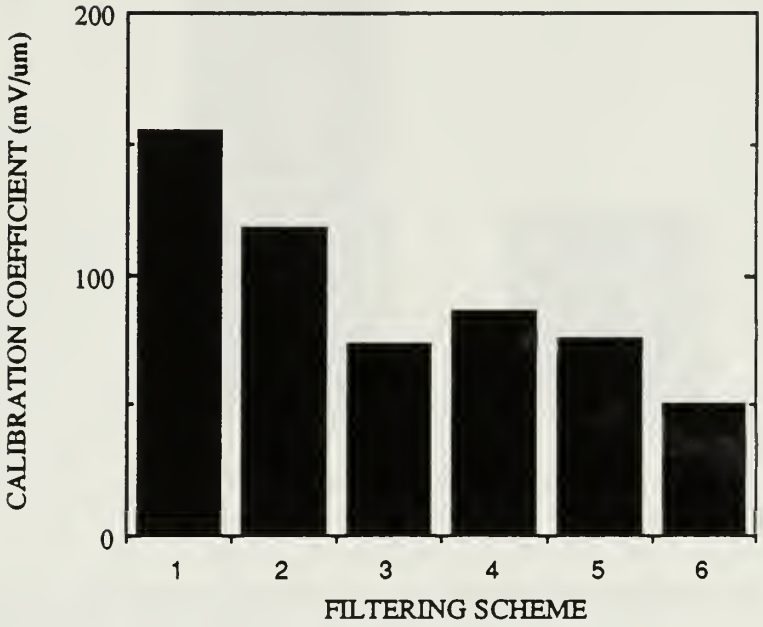

Figure 37: Motored calibration coefficients for various filtering schemes.

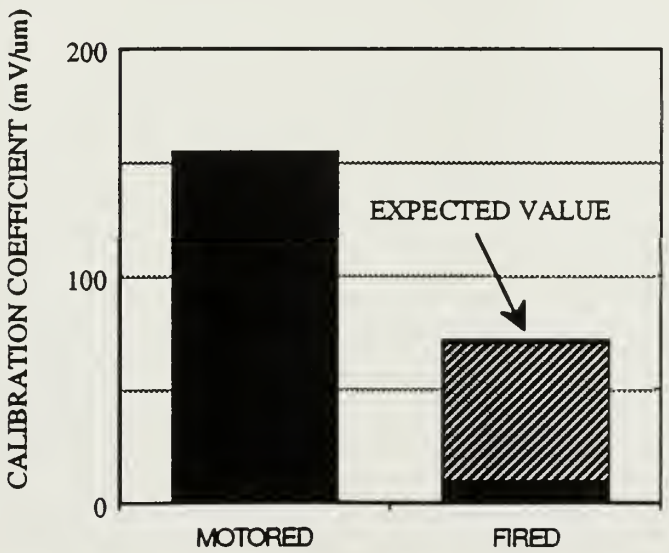

Figure 38: Reduction in calibration coefficient between motored and fired fiber optics data. Reduction is 93%.

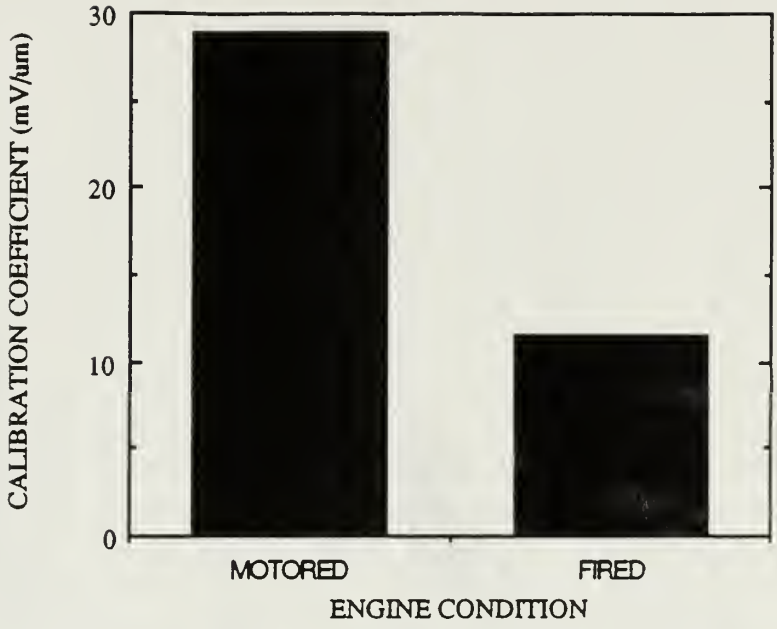

Figure 39: Reduction in calibration coefficient between motored and fired conventional optics data. Reduction is 60%.

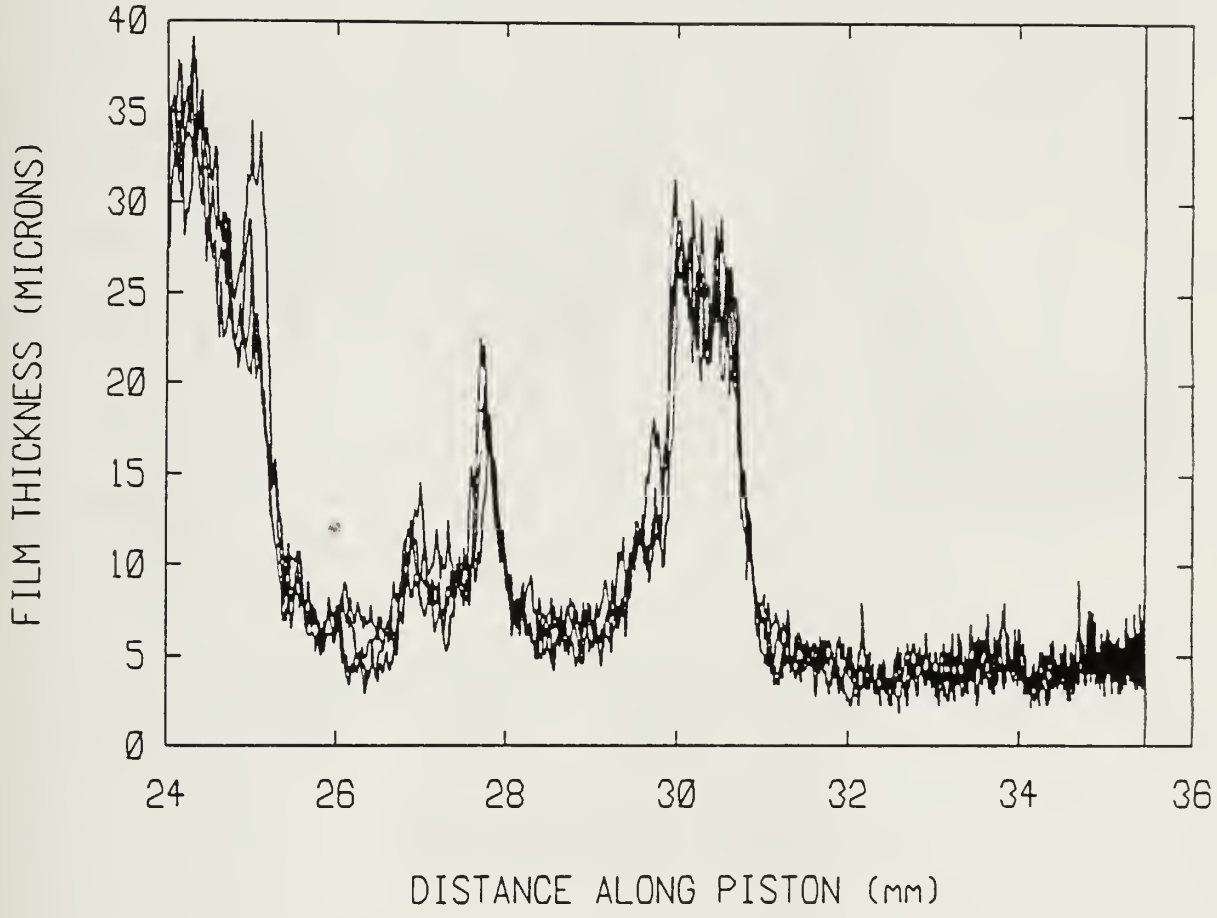

Figure 40: Detail of fired film trace in etch mark region from conventional optics data. Trace represents an overlay of 4 consecutive compression strokes, direction of piston travel is right to left.

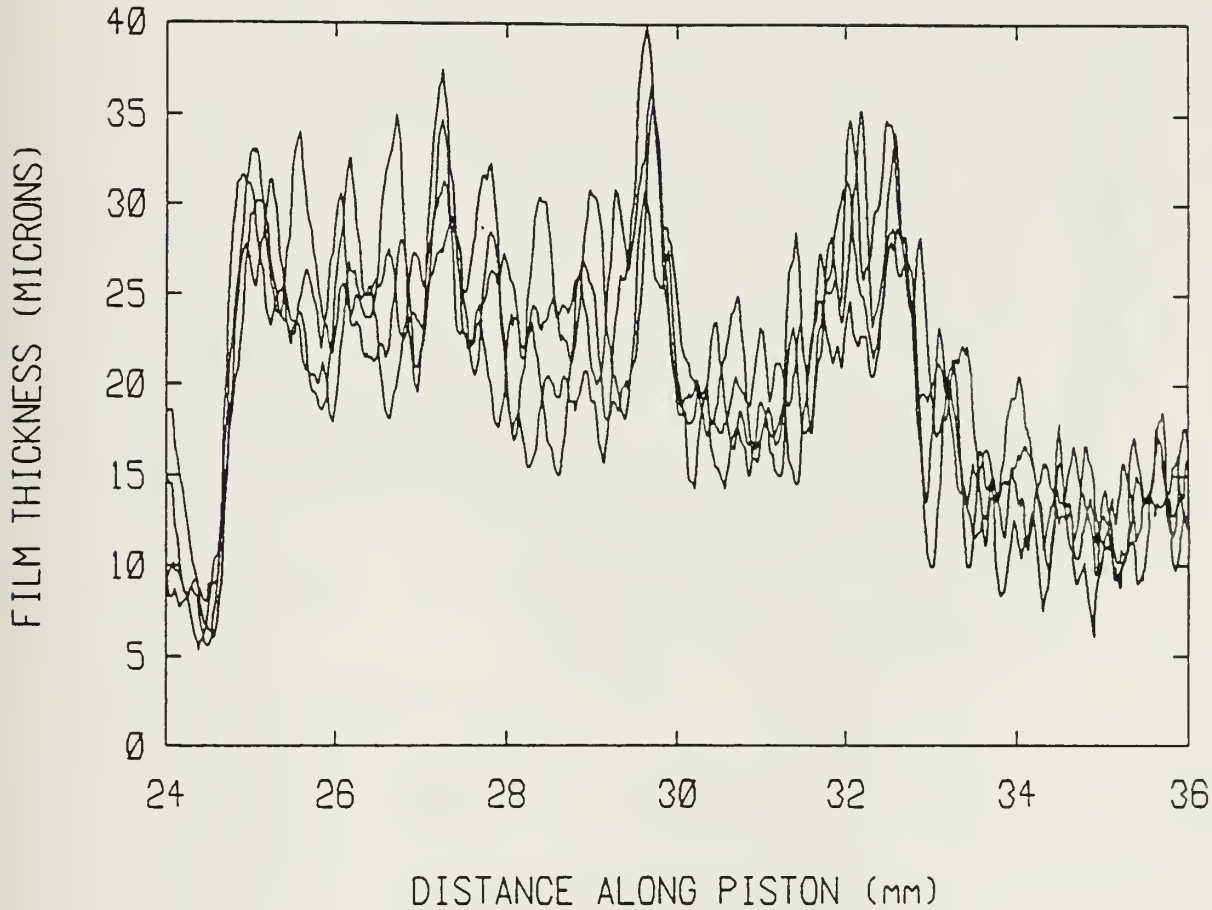

Figure 41: Detail of fired film trace in etch mark region from fiber optics data. Trace represents an overlay of 4 consecutive compression strokes, direction of piston travel is right to left.

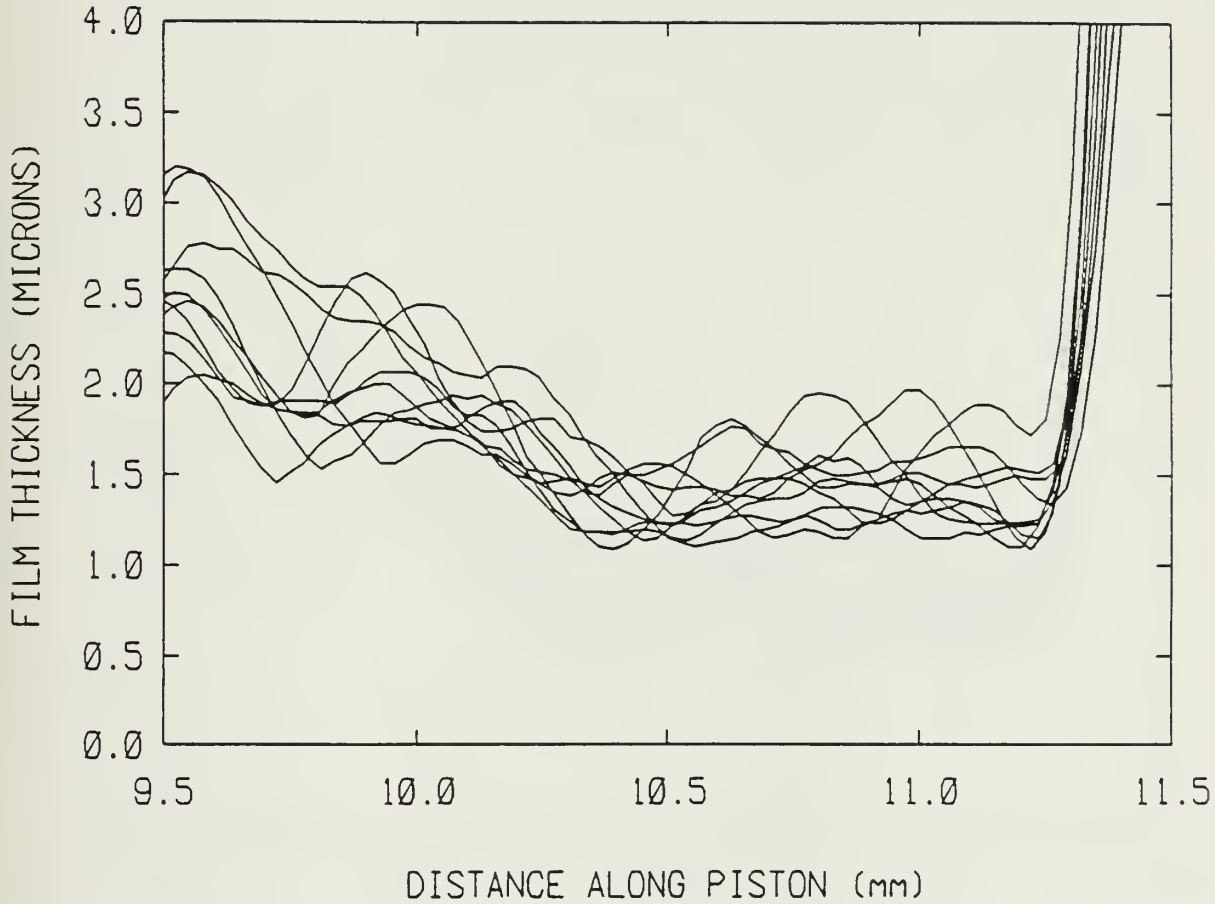

Figure 42: Detail of motored film trace in top ring region from fiber optics data. Filtering is zero 442 nm filters and one 500 nm filter. Trace represents an overlay of 10 consecutive compression strokes, direction of piston travel is right to left.

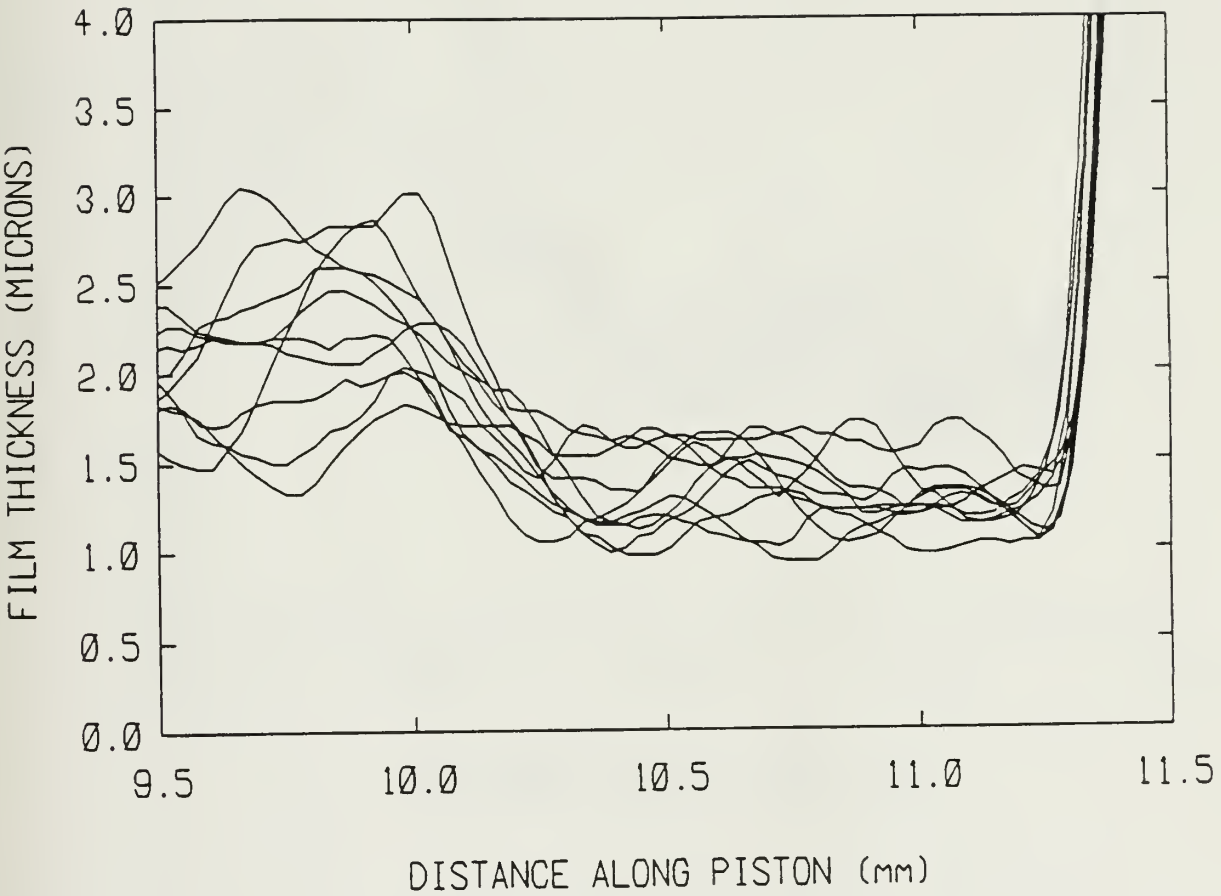

Figure 43: Detail of motored film trace in top ring region from fiber optics data. Filtering is one 442 nm filter and one 500 nm filter. Trace represents an overlay of 10 consecutive compression strokes, direction of piston travel is right to left.

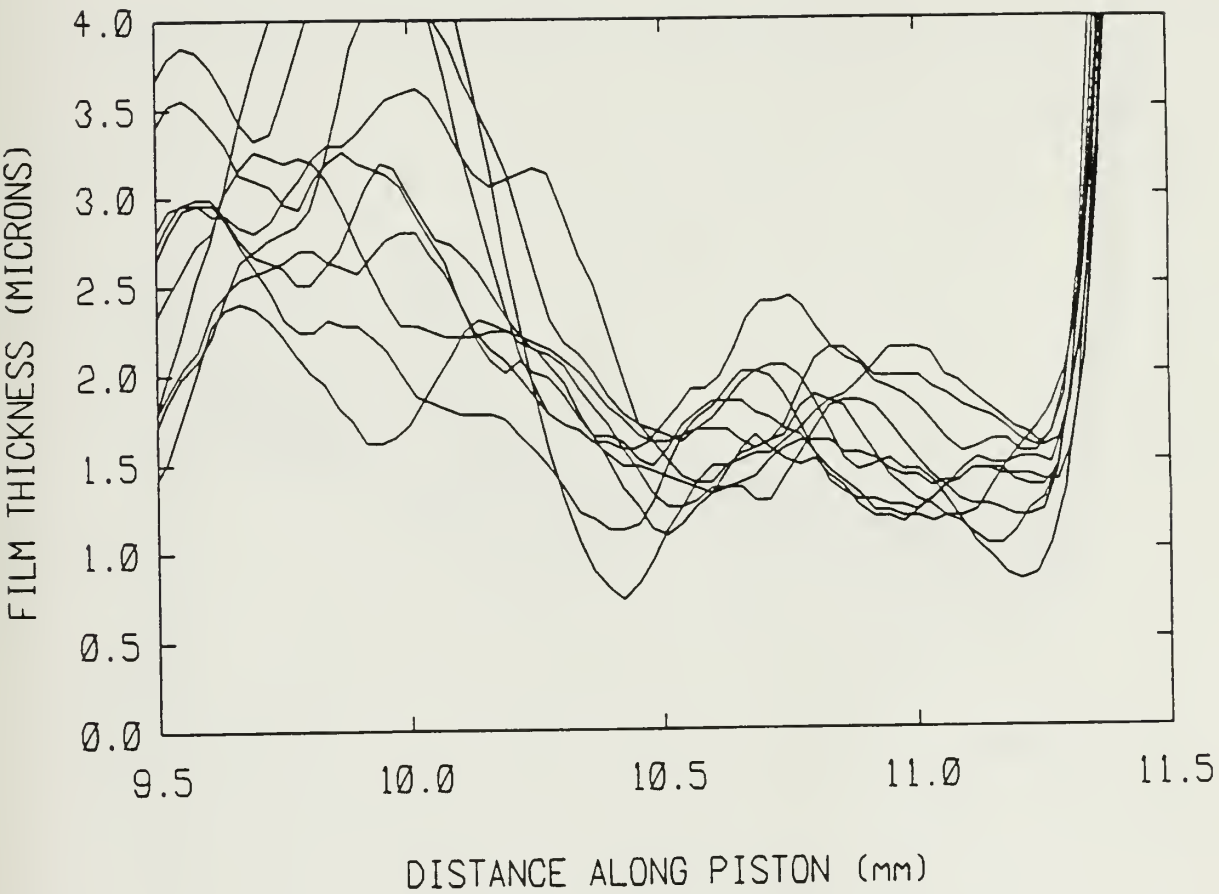

Figure 44: Detail of motored film trace in top ring region from fiber optics data. Filtering is two 442 nm filters and one 500 nm filter. Trace represents an overly of 10 consecutive compression strokes, direction of piston travel is right to left.

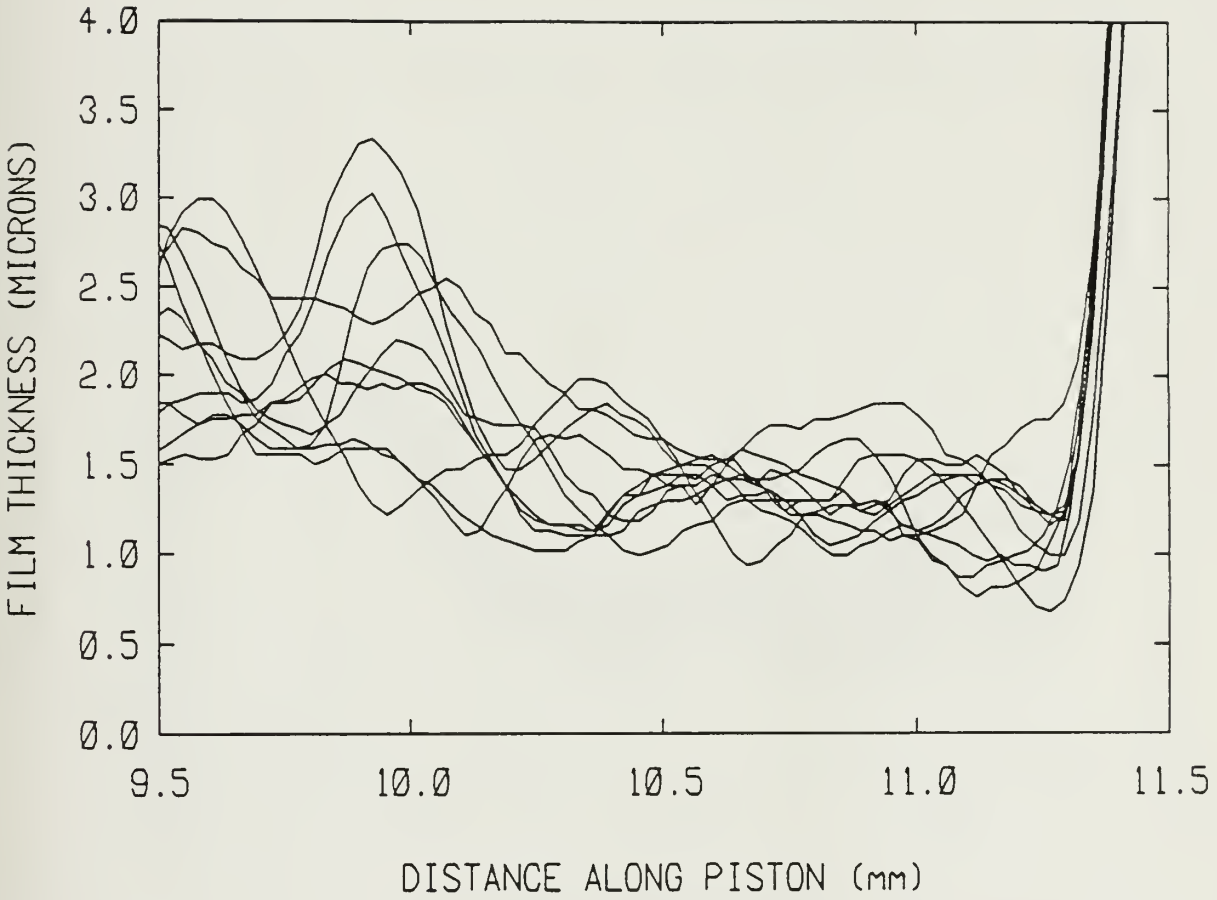

Figure 45: Detail of motored film trace in top ring region from fiber optics data. Filtering is zero 442 nm filters and two 500 nm filters. Trace represents an overlay of 10 consecutive compression strokes, direction of piston travel is right to left.

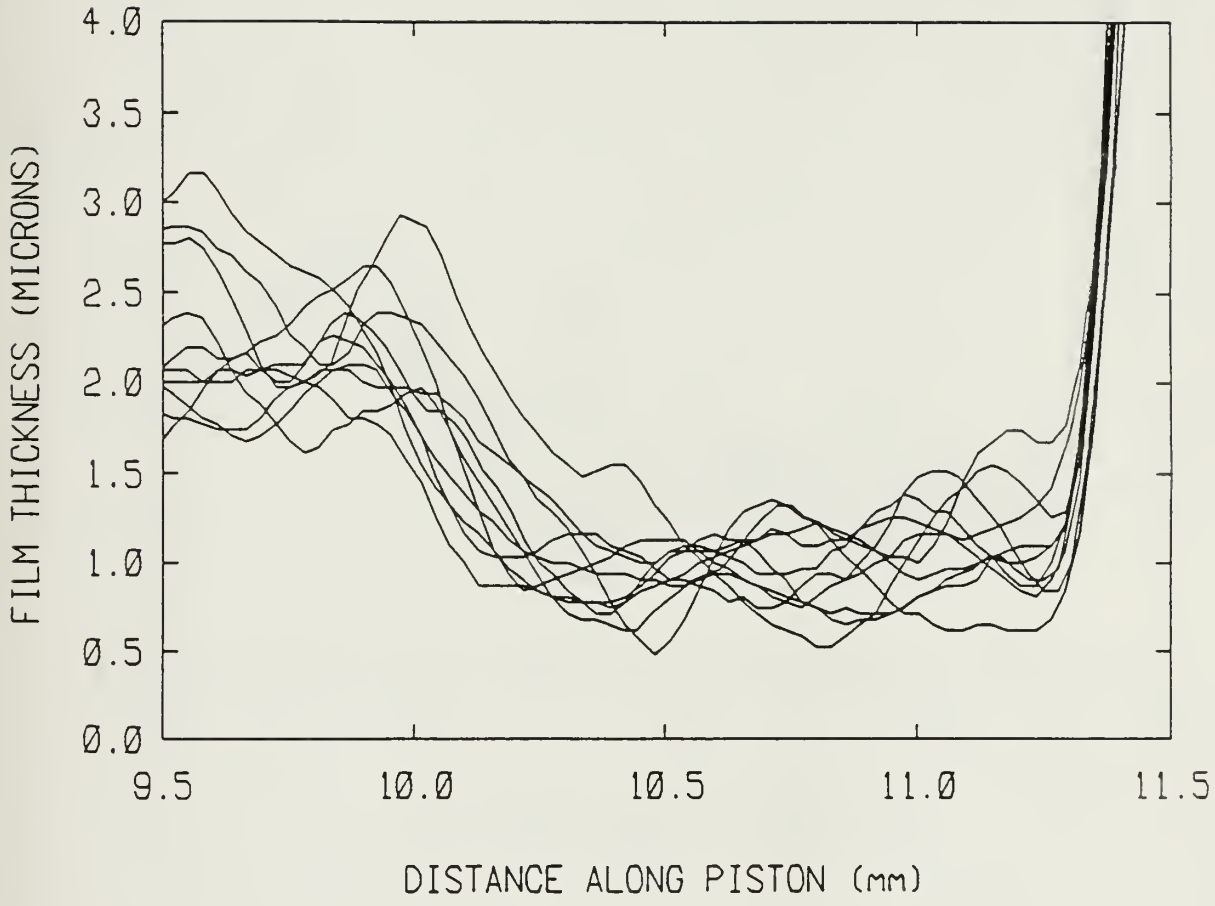

Figure 46: Detail of motored film trace in top ring region from fiber optics data. Filtering is one 442 nm filter and two 500 nm filters. Trace represents an overlay of 10 consecutive compression strokes, direction of piston travel is right to left.

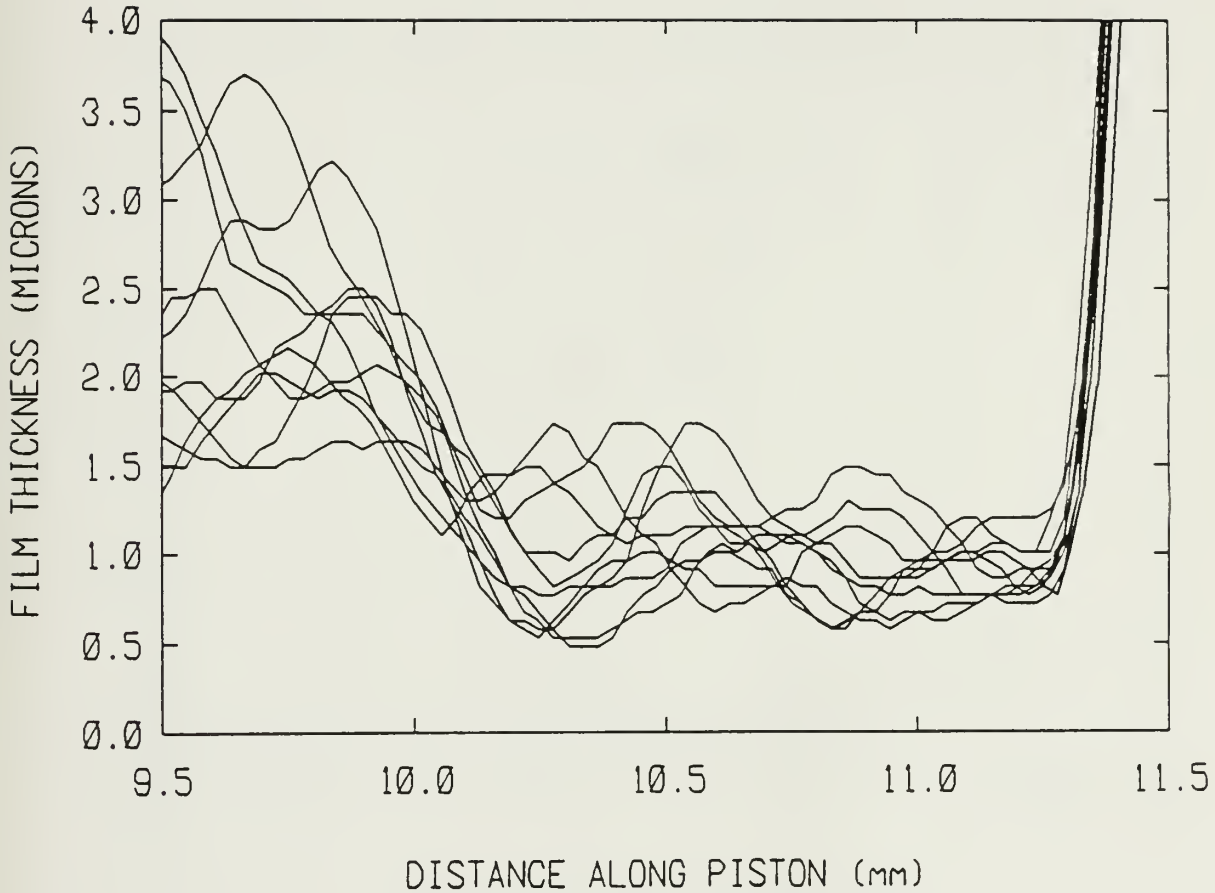

Figure 47: Detail of motored film trace in top ring region from fiber optics data. Filtering is two 442 nm filters and two 500 nm filters. Trace represents an overlay of 10 consecutive compression strokes, direction of piston travel is right to left.

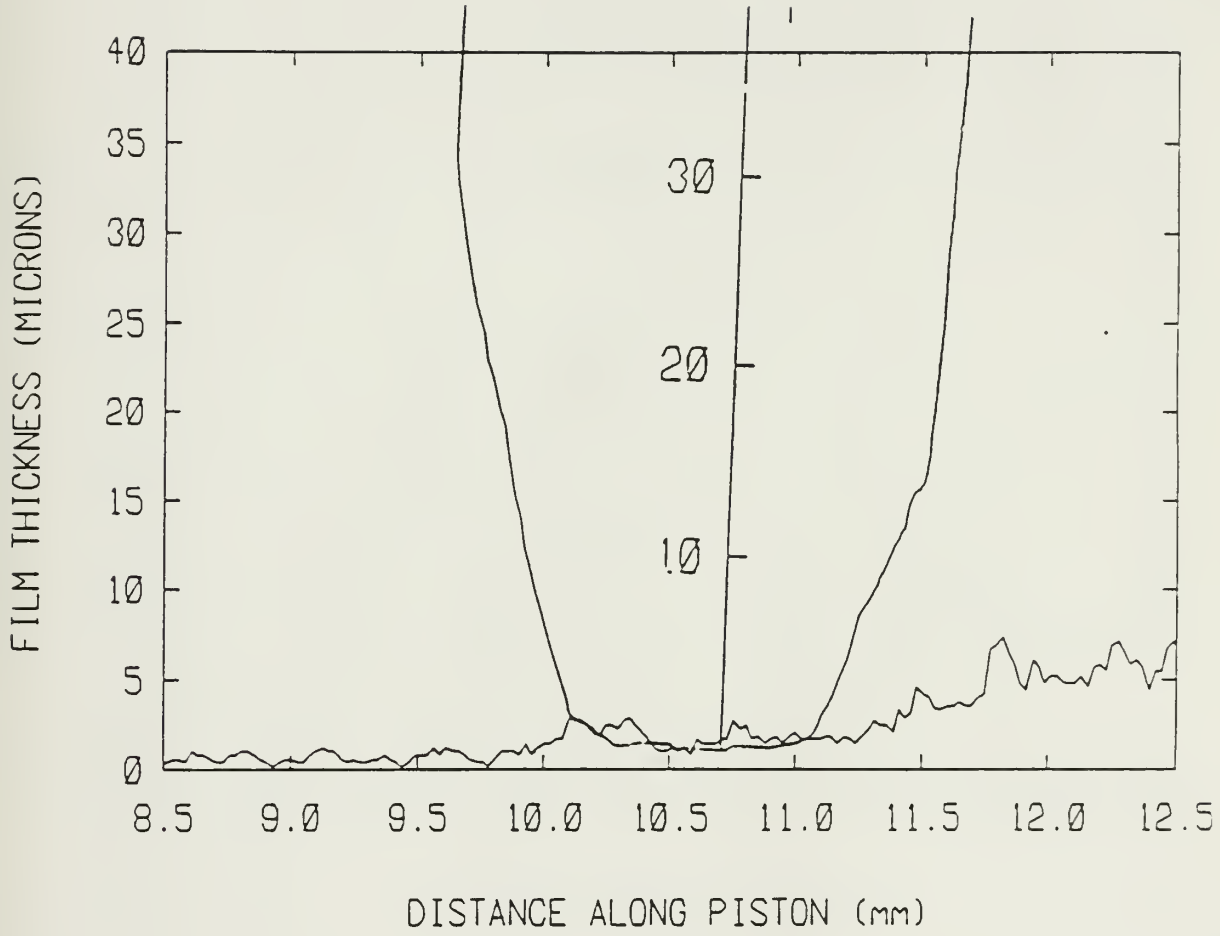

Figure 48: Typical top ring fit for conventional optics data. Randomly selected compression stroke, direction of piston travel is right to left.

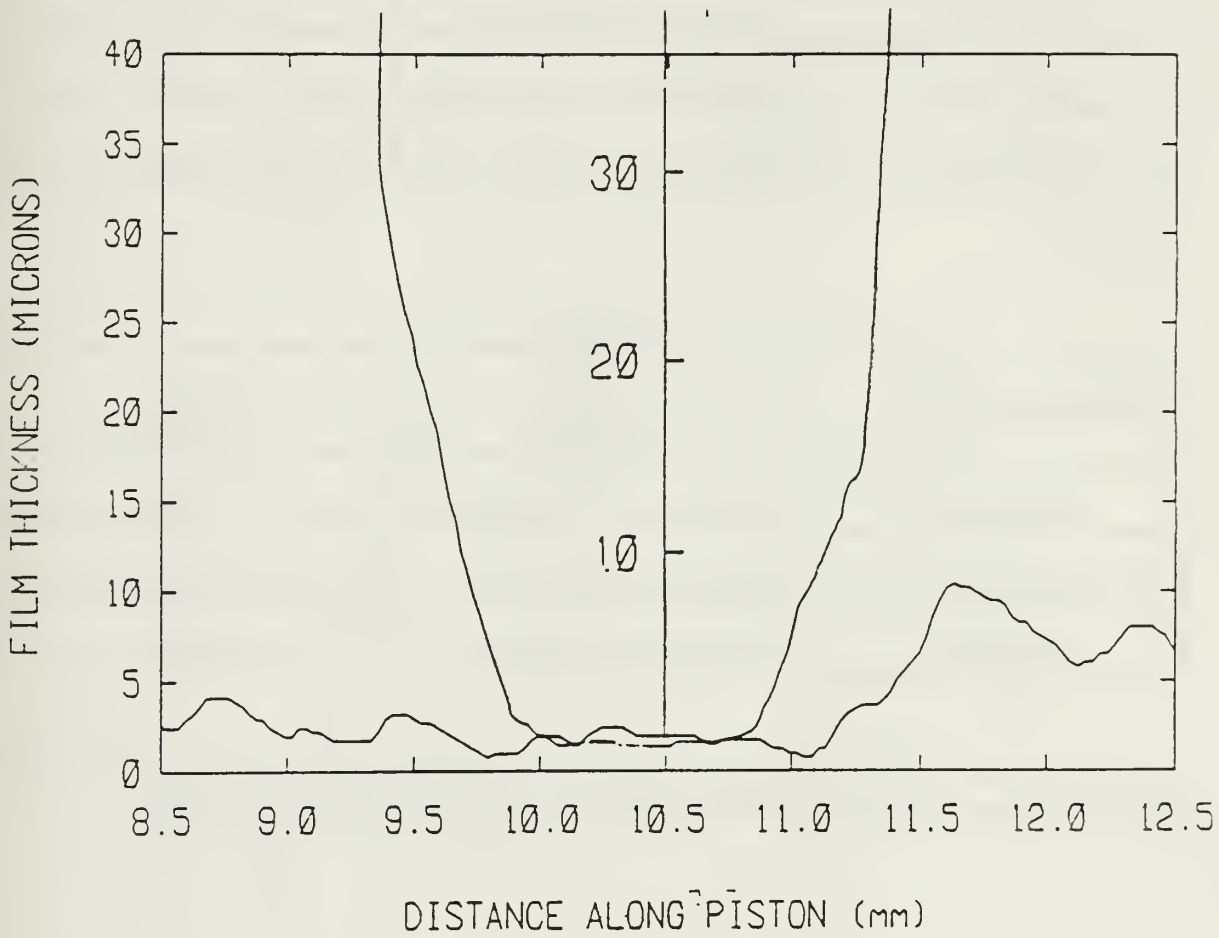

Figure 49: Typical top ring fit for fiber optics data. Randomly selected compression stroke, direction of piston travel is right to left.

FIBER "A"

INPUT LEG (POWER)	OUTPUT LEGS (POWER)	LOSS/ SPLITTING
1 (8.3 mW)	2 (2.2 mW) 3 (2 mW)	51 % / 52-48
2 (8.2 mW)	1 (2.0 mW) 3 (.039 mW)	50 % / 2-98
3 (8.2 mW)	1 (1.7 mW) 2 (.033 mW)	58 % / 2-98

FIBER "B"

INPUT LEG (POWER)	OUTPUT LEGS (POWER)	LOSS / SPLITTING
1 (8.2 mW)	2 (1.9 mW) 3 (2 mW)	48 % / 49-51
2 (8.4 mW)	1 (1.8 mW) 3 (.04 mW)	57 % / 2-98
3 (8.2 mW)	1 (1.8 mW) 2 (.038 mW)	55 % / 2-98

Figure 50: Junction and splitting losses for two different fused fiber couplers. Input leg refers to the leg of the fiber into which the laser is coupled. Two fibers of similar construction were evaluated.

Thesis
I44
c.1

Ingles
Instrumentation of a diesel engine for oil film thickness measurements using fiber optics and laser fluorescence.